

MACHINING EFFECTS ON TENSILE AND FATIGUE  
BEHAVIOR IN A  $[(\pm 45/0/90/0)_2 / \overline{0}]_s$  GRAPHITE  
EPOXY LAMINATE

By

JOHN W WEDEKING

Bachelor of Science in Mechanical Engineering

Oklahoma State University

Stillwater, Oklahoma

December 1993

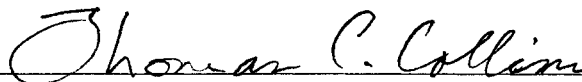
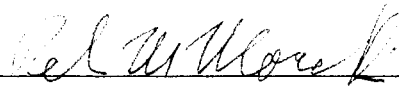
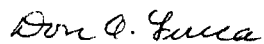
Submitted to the Faculty of the  
Graduate College of the  
Oklahoma State University  
in partial fulfillment of  
the requirements for  
the Degree of  
MASTER OF SCIENCE  
December, 1995

MACHINING EFFECTS ON TENSILE AND FATIGUE  
BEHAVIOR IN A  $[(\pm 45/0/90/0)_2/\bar{0}]_s$  GRAPHITE  
EPOXY LAMINATE

Thesis Approved:



Thesis Adviser



Dean of the Graduate College

## ACKNOWLEDGMENTS

I wish to express my sincere appreciation to my advisor, Dr. Price for his constructive guidance, patience and support. My sincere appreciation extends to my other committee members Dr. Lucca and Dr. Moretti for their assistance. I would also like to thank Mr. James Davis for his assistance in the north lab, and Mr. Makaram Raghunandan for the CNC milling work.

## TABLE OF CONTENTS

Chapter	Page
1. INTRODUCTION .....	1
Background .....	1
Objectives .....	4
2. REVIEW OF THE LITERATURE.....	5
3. EXPERIMENTAL PROCEDURE .....	10
Material .....	10
Specimen Preparation .....	12
Test Methods.....	14
4. RESULTS .....	17
Machining .....	17
Strength Testing .....	31
Scanning Electron Microscopy .....	45
5. DISCUSSION .....	53
6. CONCLUSIONS AND RECOMMENDATIONS.....	58
Conclusions.....	58
Recommendations.....	60
REFERENCES.....	61
APPENDIX A--TESTING SUMMARY .....	65

## LIST OF TABLES

Table	Page
I. Nominal Properties of Epoxy Resin .....	10
II. Nominal Properties of T300 Graphite Fiber .....	11
III. Damage comparison between HSS and carbide bits based upon length of damage away from hole .....	29
IV. Damage comparison between HSS and carbide bits based upon the percentage of hole area blocked by protruding fibers .....	30
V. Tensile strengths of specimens drilled with different feed rates. Tensile testing performed at a head rate of .0508 mm/s or a strain rate of $8.5 \times 10^{-3}$ mm/mm/s.....	31
VI. Tensile test summary .....	33
VII. Residual strength tests at constant feed rate of .153 m/min and a constant head rate of .051 mm/s which corresponds to a strain rate of $3.33 \times 10^{-4}$ mm/mm/s.....	34
VIII. Data for effect of head rate on residual strength.....	36
IX. Effect of cyclic load level on residual strength. ....	38
X. Residual strength data at various feed rates. Cyclic testing performed at $0.93 S_m$ loading at a frequency of 9 Hz.....	39

## LIST OF FIGURES

Figure	Page
1. A schematic depiction of delamination in laminate composites. ....	2
2. Laminate stacking sequence. ....	11
3. Dimensions of tensile and fatigue specimens. (Scale 1 mm = 1/2 mm).....	12
4. Specimen marking scheme. ....	13
5. Drilling fixture. (Scale 1 mm = 2 mm).....	14
6. Entry face of H1-A-1 drilled at .0178 m/min feed with HSS bit. Note that the major damage seen is from the exit face.....	19
7. Exit face of H1-A-1 drilled at .0178 m/min feed with HSS bit.....	19
8. Entry face of H2-B-6 drilled at .0508 m/min feed with HSS bit. Note that major damage seen is from the exit face.....	20
9. Exit face of H2-B-6 drilled at .0508 m/min feed with HSS bit.....	20
10. Entry face of H3-C-9 drilled at .153 m/min feed with HSS bit. Note that major damage seen is from the exit face.....	21
11. Exit face of H3-C-9 drilled at .153 m/min feed with HSS bit.....	21
12. Entry face of H4-D-13 drilled at .457 m/min feed with HSS bit. Note that major damage seen is from the exit face.....	22
13. Exit face of H4-D-13 drilled at .457 m/min feed with HSS bit.....	22
14. Entry face of H5-E-18 drilled at 1.37 m/min feed with HSS bit.....	23
15. Exit face of H5-E-18 drilled at 1.37 m/min feed with HSS bit.....	23
16. Exit face of C1-A-19 drilled at .0178 m/min feed with carbide bit.....	24
17. Exit face of C1-B-20 drilled at .0508 m/min feed with carbide bit.....	24

18. Exit face of C1-C-21 drilled at .153 m/min feed with carbide bit.....	25
19. Exit face of C1-D-22 drilled at .457 m/min feed with carbide bit.....	25
20. Entry face of C1-E-23 drilled at 1.37 m/min feed with carbide bit.....	26
21. Exit face of C1-E-23 drilled at 1.37 m/min feed with carbide bit.....	26
22. Edge view of cutting edge on new HSS drill bit .....	27
23. Edge view of cutting edge on used HSS bit. Note minor pitting when compared with Fig. 22.....	28
24. Lowest feed (.0178 m/min) chips which are a fine powder.....	28
25. Highest feed (1.37 m/min) chips which range from 1 ~ 4 mm in size .....	29
26. Damage comparison between HSS and carbide bits based upon the length of damage away from hole. ....	29
27. Damage comparison between HSS and carbide bits based upon percentage of hole area blocked by protruding fibers. ....	30
28. Effect of feed rate on tensile strength. All tensile tests performed at .051 mm/s head rate.....	32
29. Tensile test results at various head rates and feed rates.....	33
30. Residual strength testing at a constant feed rate of .153 m/min and a constant head rate of .051 mm/s which corresponds to a strain rate of $3.33 \times 10^{-4}$ mm/mm/s.....	34
31. Percent increase in residual strength.....	35
32. Effect of head rate on residual strength. ....	36
33. Comparison of residual strength increase at different head rates. ....	37
34. Effect of cyclic load level on residual strength. ....	38
35. Effect of feed rate on residual strength.....	39

36. Temperature Profile for 10,000 cycles at 9 Hz. Data taken from specimens H9-C-36 and H9-C-37.	40
37. Temperature Profile of 380,000 cycles at 9 Hz. Data taken from specimen H8-C-35.	41
38. H6-C-27 tensile tested at .004 mm/s head rate. Note uniform and even fracture surface except for 45° ply which did not fracture	42
39. H7-C-28 tensile tested at 20.3 mm/s head rate. Note uniform and even fracture surface except for 45° ply which did not fracture	42
40. H3-C-10 fatigued at 27.9 KN for 1,150,855 cycles. Residual strength was 32.2 KN. View is looking down on bit entry. Note rough and uneven fracture surface	43
41. H7-C-29 fatigued at 27.9 KN for 1,100,000 cycles. Residual strength was 36.1 KN. View is looking down on bit entry. Note rough and uneven fracture surface	43
42. Side view of H3-C-10. Note brooming effect at left and ply separation in middle of thickness at right	44
43. SEM view description.	45
44. Edge view taken from H3-C-28 which was drilled at .153 m/min feed. Specimen was tensile tested at 20.3 mm/s head rate which corresponds to head rate during a 9 Hz fatigue test.	47
45. Edge view taken from H6-C-27 which was drilled at .153 m/min feed. Specimen was tensile tested at slow head rate of .004 mm/s.	47
46. Fracture surface view of H3-C-28. Upper half of picture is 90° fibers while lower half is 0° fibers. Specimen experienced fast strain rate tensile test	48
47. Fracture surface view of H6-C-27. Upper half is 0° fibers while lower portion is 90° fibers. Specimen experienced slow head rate tensile test	48
48. Fiber detail taken from fracture view of specimen H6-C-27. Specimen was tensile tested at slow head rate	49
49. Machined surface view of specimen H3-C-28. Specimen drilled at .153 m/min feed. Specimen experienced fast strain rate tensile test.	49



50. Edge view taken from H7-C-29 which was drilled at .153 m/min feed. Specimen experienced 1,100,000 cycles at 27.9 KN. Residual strength was 36.1 KN .....50
51. Edge view taken from H5-E-15 which was drilled at 1.37 m/min feed. Specimen experienced 10,010 cycles at 27.9 KN. Residual strength was 32.9 KN .....50
52. Machine surface detail from H7-C-29. Top bit entry at .153 m/min feed. 1,100,000 cycles at 27.9 KN resulted in a residual strength of 36.1 KN .....51
53. Machined surface view from H5-E-15. Bottom bit entry at 1.37 m/min feed. 10,010 cycles at 27.9 KN resulted in a 32.9 KN residual strength.....51
54. Edge view taken from H2-B-7 which was drilled at .0508 m/min feed. Specimen was tensile tested at .051 mm/s head rate with a strength of 29.8 KN. ....52
55. Fracture surface detail of H7-C-29. Upper half is 0° fibers while lower portion is 90° fibers. 1,100,000 cycles at 27.9 KN resulted in a 36.1 KN residual strength ....52

## CHAPTER 1

### INTRODUCTION

Composite materials are used in many high performance applications because of their superior strength-to-weight and stiffness-to-weight ratios. The use of composites in aerospace and aeronautical structures has typically resulted in improved structural performance, but the fabrication cost is higher as compared to conventional metallic structures [1]. Many researchers have studied composite material mechanics and behavior, but little research has been done in the area of composite machining [2] and the resulting residual strength after fatigue testing [3]. The following research will investigate both machining and residual strength testing of a quasi-isotropic laminate.

#### Background

Several new nontraditional machining processes, including ultrasonic machining, water jet machining, electro-discharge machining, and laser beam machining are being used to machine composites. Nevertheless, conventional machining processes such as drilling, routing, sawing and milling continue to be widely used [4]. Drilling of composites is still a common operation in the aerospace industry. Unfortunately, a

number of problems, including delamination, fiber breakout and fraying are introduced during drilling. These defects are unique to fiber composites and are not seen in homogeneous materials.

Delamination is generally regarded as one of the most frequent flaws encountered during drilling [5]. Drilling delamination is a matrix dominated failure behavior which commonly occurs in the interply region. The delamination appears as a peeling away of the bottom ply or plies as a result of the drill pushing the layers apart before cutting through them. Fig. 1 displays delamination in a laminate.

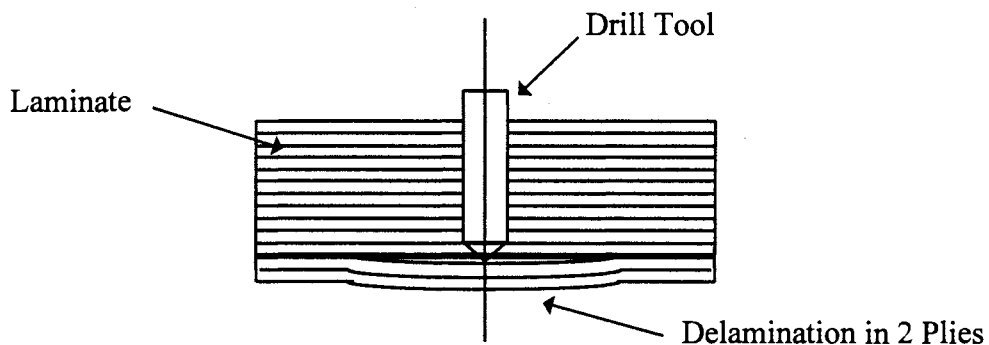


Figure 1: A schematic depiction of delamination in laminate composites.

Although not shown in Fig. 1, similar but less severe delamination also occurs at drill entry due to drill tool pullout. When subjected to compressive, shear or cyclic loads, delamination can be a limiting factor [4].

Delamination is usually greater at the drill exit side where the damage often extends into many layers of the laminate. Composite failure can be a result of the

propagation of these interlaminar cracks. X-radiography, optical and ultrasonic techniques are commonly used to observe the delamination damage, but since damage is not uniform, problems can arise. One alternative to these non destructive techniques is to perform mechanical tests on damaged material and observe how it effects the tensile and residual strength of the material.

Drilling feed rate, speed and tool geometry all affect the amount of damage introduced during drilling. Although not always practical, the use of backing pressure also reduces drilling damage [6,7].

Graphite/epoxy composites are beginning to be utilized by commercial revenue producing aircraft. Design of structural components in commercial aircraft is primarily dominated by the requirement of long service life. It has been documented that commercial airplanes can accumulate up to 60,000 service hours. Although some military cargo planes log up to 50,000 service hours, they only encounter about half as many landings as a commercial plane [8]. Landings produce the greatest amount of fatigue stresses. With nearly a million rivets in a single aircraft, it is easy to recognize the importance of understanding the fatigue resistance properties of composites with holes.

## Objectives

The primary objective of this study is to investigate the damage introduced into a graphite/epoxy continuous fiber composite during drilling and its effects on the strength of the composite. More specifically the objectives are:

1. Investigate damage introduced during drilling of a graphite/epoxy laminate and the effect of the damage on the material's strength.
2. Quantify the effects of fatigue testing on residual strength.
3. Compare and contrast the differences between a thermosetting graphite/epoxy composite and a thermoplastic PPS/E-glass composite with respect to machining induced damage and the resulting strength.

To drill holes in each of the specimens a CNC milling machine, capable of a wide range of feed rates, was used. During the conceptual phase of research, feed rates of .0178, .0508, .153, .457, and 1.37 m/min were selected. The drilling speed was kept at a constant 2,000 rpm and all holes were drilled without a backing plate to ensure maximum damage [7]. A number of static tensile tests and residual strength tests were performed on the drilled specimens. Residual strength refers to performing a static tensile test on a sample with a previous fatigue history. This fatigue history was acquired by load control of tension-tension fatigue tests performed on an Instron 8500.

## CHAPTER 2

### REVIEW OF THE LITERATURE

Study in the area of composite damage began in early 1970. Methodology and experimental results of X-ray nondestructive testing techniques and acoustic emission monitoring was performed by Chang et. al. [9]. Compression fatigue tests on a quasi-isotropic graphite/epoxy composite were performed by Ryder and Walker [10] while notched and unnotched fatigue tests were performed on an angle-ply graphite epoxy [11]. Tests on the ultimate strength of a quasi-isotropic  $[0^\circ/\pm 45^\circ/90^\circ]_{2S}$  laminate with a hole were also conducted by Lee and Mall [12].

Recently, studies concerning drilling delamination have been conducted. Ho-Cheng and Dharan [2] developed an analytical model which predicts the optimal thrust force as a function of drilled hole depth. Jain and Yang [4] also developed a similar model based on thrust force to predict the critical thrust force and feed rate at which delamination cracks begin to propagate. In addition to their analytic model, Jain and Yang suggest variable feed rates and bits with small chisel edges to avoid delamination. They also discovered that point angle of the bit is of secondary importance.

Other related machining research was performed by Ho-Cheng, et. al [13]. They studied machinability including chip characteristics, drilling force, surface roughness, and edge integrity as an effect of feed rate, cutting speed, drill geometry, and lay-up system on both thermoset and thermoplastic based composites. One result of interest is that at high cutting speeds and low feed rate, tool tip heating promotes polymer plasticity which results in ribbon like chips. They also noted that large feed rates produce large chips. Colligan and Ramulu [14] assessed the influence of drill feed rate, cutting speed, coolant application, bit geometry and cutting edge wear on the formation of pits during machining of graphite/epoxy panels.

In early 1980, Pengra and Wood [5] were the first to study the influence of hole quality on composite fatigue behavior. After developing a pin bearing static and cyclic test to evaluate the influence of hole flaws on a 5208/T300 graphite/epoxy laminate, they discovered that delamination of the exit face ply during hole fabrication did not influence static pin bearing strength or the bearing endurance limit. This is surprising since Butler, et. al. [15] found that fatigue life is dependent upon the surface quality of the exposed edge. Polishing the edge increased the fatigue life by presumably removing potential cracks. Curtis [16] increased the fatigue life of specimens by introducing slots into the ends of the test coupon. It was concluded that the slots increased fatigue life by shifting the failure zone away from the complex stress field in the edge region to a region where simple shear is encountered.

A background in failure mechanisms and fractography is also needed for this study. Layer cracking, delamination, fiber breakage, and fiber-matrix interfacial

debonding are the four basic failure mechanisms in composites [17]. Any combination of these mechanisms can cause failure. Additionally, unidirectional composites have three failure modes which include: (1) brittle failure; (2) brittle failure with fiber pull-out; and (3) brittle failure with debonding and/or matrix failure [18]. Variations in laminate stacking sequence can lead to differences in failure mode. Typically  $[0^\circ/\pm 45^\circ/90^\circ]_s$  laminates fail along a line perpendicular to the load while  $[\pm 45^\circ/90^\circ/0^\circ]_s$  laminates fail along a line  $45^\circ$  to the loading [19]. When studying a composite fracture surface there are three basic fracture types. These include interlaminar (failures between plies), intralaminar (fractures located internally within a ply) and translaminar (fractures oriented transverse to the fracture plane) [20].

Prior to the present study, Nayak [21], Powers [22] and Hegde [7] conducted similar tests on a PPS/glass fiber composite. From their studies they found the following:

1. Tensile strength increases with increasing strain rate.
2. Tensile strength is not effected by variations in drilling feed rate from 0.0015 ipr to 0.006 ipr.
3. Use of a backing plate reduces damage during drilling.
4. Fatigue life is decreased as feed rate increases when holes are drilled without a backing plate.
5. Fatigue behavior may be influenced by strain hardening of the matrix.
6. Residual strength decreased with cyclic axial fatigue testing.



Powers [22] noted longitudinal crazing cracks which occurred during fatigue testing. Longitudinal cracks originating from the hole were also documented by Schutz [23] for graphite epoxy specimens.

Previous research in the area of composite fatigue testing procedures was also found. Mehran [24] found that during dynamic testing of a composite, gain is related to the total damage while phase may be related to the damage rate. Ryder [10] observed that visible delamination did not always occur during tension-tension (T-T) fatigue tests, but when such delamination did occur, the remaining lifetime of cycles could be large or small. Thus he concludes that delamination may be a more useful definition of failure. Ryder also noted that the coupon remained at room temperature until the specimen cycle count reached was approximately equal to the count when delamination was noted. At this point the temperature quickly rose 8 °C and remained constant until failure. In other studies, Curtis [16] determined that this heating could be a result of either hysteresis or frictional heating. Curtis also documented that little hysteresis heating occurred in laminates dominated by continuous fibers in the test direction (due to small strains). With this type of a specimen, dynamic testing at 10 Hz is acceptable. Conversely, laminates with fewer fibers in the test direction produced larger strains and a frequency of 5 Hz was needed to prevent heating.

Residual strength tests on composites with a fatigue history were conducted by a few researchers. Sendekyj [25] recorded the residual strength after conducting room temperature T-T fatigue tests on samples with a central notch. He found that the central notch is correlated with the size of the fatigue induced matrix damage. If the fatigue

induced matrix damage zone is the same size or smaller than the delamination region observed in the static tests prior to failure, then the residual strength is equal to the static strength. Conversely, if the size of the fatigue induced matrix zone is much larger than the delamination zone in the static test, the residual strength is higher than the static strength. Awerbuch [26] found that residual strength testing on off-axis graphite epoxy samples did not exhibit any reduction in residual strength after performing 100,000 cycles. Additionally, it is generally argued that fatigue failure occurs when residual strength becomes equal to the strength level of the fatigue test [3].

## CHAPTER 3

### EXPERIMENTAL PROCEDURE

#### Material

All tests were performed on an graphite epoxy panel which was hot compression molded to navy specifications by Kinetic Composites Incorporated. Each of the plies were unidirectional T300 graphite while the matrix was a 120 °C (250 °F) epoxy resin. Tables 1 and 2 present the properties of the graphite fibers and the epoxy matrix.

Table 1: Nominal Properties of Epoxy Resin [27]

Matrix Property	Value
Density	1.22 Mg/m <sup>3</sup> (.044 lb/in <sup>3</sup> )
Tensile Strength	103 MPa (15 ksi)
Modulus	3.4 GPa (0.5 · 10 <sup>6</sup> psi)
Poisson's Ratio	0.35
Heat Capacity	1047 J/kg · °C (0.25 Btu/lb · °F)
Heat Conductivity	0.18 W/m · °C (1.25 Btu · in/ft <sup>2</sup> · hr · °F)
Thermal Expansion Coefficient	0.65 · 10 <sup>-6</sup> m/m · °C (36 · 10 <sup>-6</sup> in/in · °F)

Table 2: Nominal Properties of T300 Graphite Fiber [28]

Fiber Property	Value
Fiber Diameter	6.93 $\mu\text{m}$ (0.273 mils)
Density	1.77 $\text{Mg/m}^3$ (.064 $\text{lb/in}^3$ )
Tensile Strength	2413 MPa (350 ksi)
Longitudinal Modulus	231 GPa ( $33.5 \cdot 10^6$ psi)
Transverse Modulus	13.8 GPa ( $2.0 \cdot 10^6$ psi)
Longitudinal Shear Modulus	9.0 GPa ( $1.3 \cdot 10^6$ psi)
Transverse Shear Modulus	4.8 GPa ( $0.7 \cdot 10^6$ psi)
Longitudinal Poisson's Ratio	0.2
Transverse Poisson's Ratio	0.25
Heat Capacity	921 $\text{J/kg} \cdot ^\circ\text{C}$ (0.22 $\text{Btu/lb} \cdot ^\circ\text{F}$ )
Longitudinal Heat Conductivity	83.6 $\text{W/m} \cdot ^\circ\text{C}$ (580 $\text{Btu} \cdot \text{in/ft}^2 \cdot \text{hr} \cdot ^\circ\text{F}$ )
Transverse Heat Conductivity	8.4 $\text{W/m} \cdot ^\circ\text{C}$ (58 $\text{Btu} \cdot \text{in/ft}^2 \cdot \text{hr} \cdot ^\circ\text{F}$ )
Long. Thermal Expansion Coefficient	$-99 \cdot 10^{-6} \text{ m/m} \cdot ^\circ\text{C}$ ( $-0.55 \cdot 10^{-6} \text{ in/in} \cdot ^\circ\text{F}$ )
Trans. Thermal Expansion Coefficient	$0.1 \cdot 10^{-6} \text{ m/m} \cdot ^\circ\text{C}$ ( $5.6 \cdot 10^{-6} \text{ in/in} \cdot ^\circ\text{F}$ )

The laminate, composed of a 0.15 mm (0.005952 in) thick JD Lincoln tape, had a total of 21 plies. The final press panel size is .9652 m x 1.27 m (38 in x 50 in) with a design thickness of 3.16 mm (0.12432 in). The laminate zero direction is in the 1.27 m (50 in) direction. The laminate orientation code is  $[(\pm 45/0/90/0)_2 / \bar{0}]_s$ . Fig. 2 shows the stacking sequence.

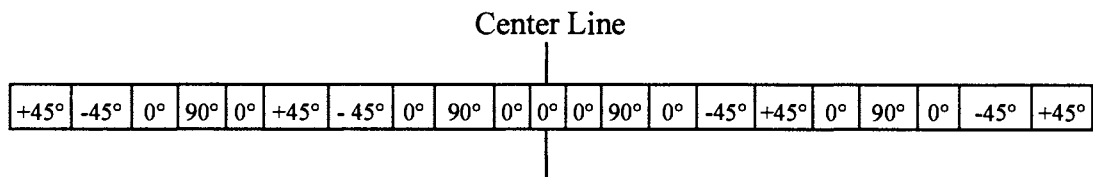


Figure 2: Laminate stacking sequence.

The laminate stacking is balanced, symmetric and quasi-isotropic. A balanced and symmetric laminate has both geometric and material properties symmetric about the

centerline. The laminate coupling stiffness matrix  $[B]$  for a symmetric laminate is always zero. Quasi-isotropic implies that it is possible to use orthotropic laminae to produce a final laminate which exhibits some elements of isotropic behavior. Thus the strength is fairly uniform in the longitudinal and transverse directions and the extensional stiffness matrix  $[A]$  is isotropic, while the other stiffness matrices  $[B]$  and  $[D]$  are not necessarily isotropic in form [27].

### Specimen Preparation

In this research, all specimens were rectangular with a hole placed at the center. Stress concentrations introduced around the hole ensured failure away from the grips. End tabs were not necessary as the specimen thickness was adequate. Fig. 3 displays the exact dimensions and geometry of each test specimen.

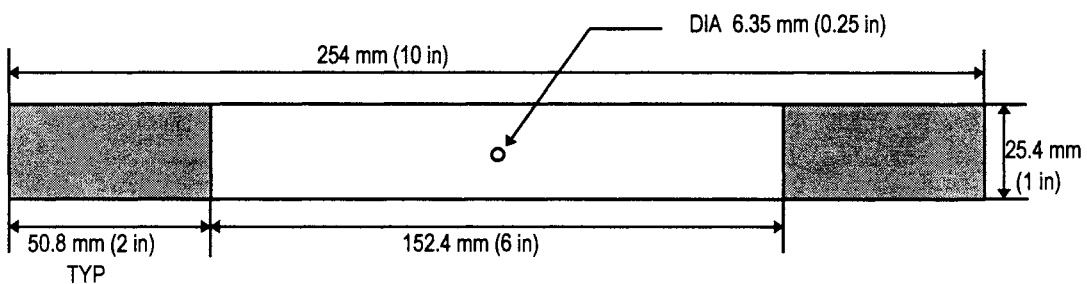


Figure 3: Dimensions of tensile and fatigue specimens. (Scale 1 mm = 1/2 mm)

The dimensions and geometry are in accordance with ASTM 3039/D 3039M-93.

Each test specimen was cut with a band saw such that the 254 mm length was aligned with the zero direction. Since the band saw produces a rough cut, each specimen was cut approximately 2.54 mm (0.1 in) over size. Final dimensions were obtained on a vertical milling machine using a fly cutter with a carbide insert. Low speeds were used on the mill and the carbide insert was periodically sharpened.

The 6.35 mm (.25 in) hole was drilled at the center of each specimen without a backing plate. Both a 118° HSS bit and a 118° split point “micrograin” carbide bit were used. A new HSS bit was used after every four holes to prevent hole damage due to bit degradation. To quickly identify each specimen, a marking code was developed. A description of the code follows in Fig. 4.

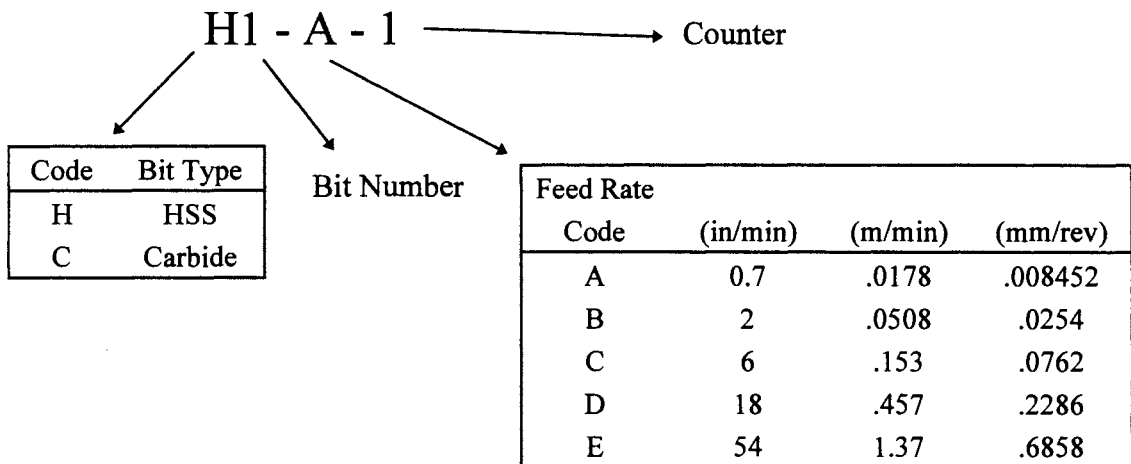


Figure 4: Specimen marking scheme.

For example, H3-C-10 was the tenth machined specimen drilled with the third HSS drill bit at a feed rate of .153 m/min. By not using a backing plate, the maximum amount of damage around each hole was obtained.

The drill speed was maintained at 2000 rpm for all holes and no coolant was used. At this speed, no coolant was needed since epoxy melting did not occur [29]. During drilling, a fixture was used to hold each specimen (see Fig. 5).

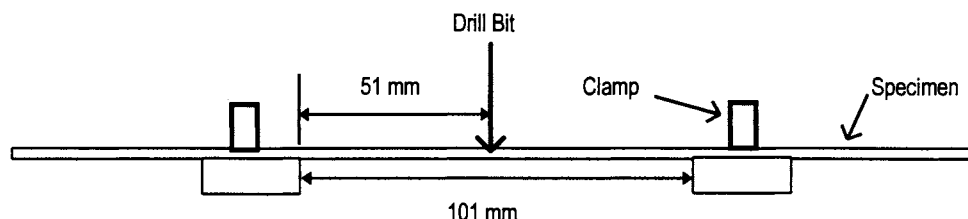


Figure 5: Drilling fixture. (Scale 1 mm = 2 mm)

Machining was performed at 24 °C with 43% humidity. The holes at .153 m/min were drilled on a variable speed vertical milling machine. All other feed rates were obtained on a Bridgeport Interact 412 three axis CNC milling machine. By programming the CNC mill a very broad range of feeds, ranging from .0178 m/min to 1.37 m/min, was obtained.

### Test Methods

Static and dynamic tests were performed on an Instron 8500. To allow for comparison with previous work, axial fatigue testing was performed. Hydraulic grips were installed on the Instron to hold the test specimens. The grips applied sufficient lateral pressure to prevent coupon slippage when a grip pressure of 10.3 MPa was used. A 1300 N pre-load was used to prevent slippage. Gauge blocks were used to align each

test specimen in the grips. Top and bottom head alignment was also performed to prevent coupon twisting.

Static tensile tests were conducted on a closed loop Instron tester under room temperature ( $\sim 25^{\circ}\text{C}$ ) and ambient humidity ( $\sim 60\%$  relative humidity) conditions. Tests were performed according to the standard test methods for tensile properties of a polymer matrix composite (ASTM D 3039/D 3039M - 93). Residual strength tests were also performed under the same standard. Both the tensile and residual strength tests were performed at a number of head rates. Head rate refers to the top head speed on the Instron tester.

Constant load T-T axial fatigue tests were also conducted on the Instron tester under the same room temperatures and conditions as the static tests. The fatigue testing was not carried out to failure since the specimens were used for residual strength testing. Tests were performed following ASTM D 3479-76 (Reapproved 1990) standard test methods for tension-tension fatigue of oriented fiber, resin matrix composites. The loading procedure is as follows: the specimen is first loaded statically in tension to some prescribed load level; it is then followed by oscillatory loading with the maximum and minimum stress amplitude level of  $R = 0.2$ . To prevent hysteresis heating, all fatigue tests were conducted at 9 Hz. The closed loop Instron tester did not reach equilibrium conditions until approximately 100 cycles, therefore 100 cycles were not included in the count of the short life fatigue tests (this is noted in Appendix A--Test Summary). The maximum cyclic stress ( $\sigma_{\max}$ ) can also be presented as percent of the mean strength from



tensile testing. For example,  $0.93 S_m$  implies a load level of 27.85 KN if the sample strength is 29.95 KN.

An Omega thermocouple thermometer was used to track the specimen's temperature. The thermocouple wires were placed inside the drilled hole at the middle of the thickness. The thermocouple had a resolution of 1 °C.

A zoom microscope was used to observe and photograph the fractured specimens. Photographs were also taken before fracture to note any differences on a macroscopic scale. To get more explicit views of the damaged hole areas and fractured surfaces a Scanning Electron Microscope (SEM) was used.

## CHAPTER 4

### RESULTS

#### Machining

Machining was documented by taking Polaroid pictures through the zoom microscope. The first group of 10 pictures (Figs. 6 ~ 15) shows the resulting damage from using a HSS bit at the five feed rates. As stated earlier, no backing plate was used for any of the holes. The results of using a carbide bit are shown in Figs. 16 to 21. The HSS bits were examined under the zoom microscope and some minor pitting was recorded (see Figs. 22 and 23).

During machining, chips were saved and their size was noted. At the lowest feed rate the chips were a fine powder (Fig 24). As the feed rate increased, the chip size also increased until 1 ~ 4 mm chips were produced at the fastest feed (Fig 25). Chip characteristics were similar for both the HSS and carbide bits.

The damage accumulation presented in the pictures (Figs. 6 ~ 21) is further quantified in two ways. First, the distance which the damage extends away from the drilled hole is presented for both the HSS and carbide bits (Table 3 and Fig. 26). Second,

the damage for both types of bits is characterized by comparing the percent of area which is covered by the  $\pm 45^\circ$  fibers which are left protruding into the hole (Table 4 and Fig 27). To calculate the percent area blocked, the area was approximately measured (in cm) from each picture. After dividing by the scale twice, the percent area was calculated based upon a hole area of  $0.32 \text{ cm}^2$ .

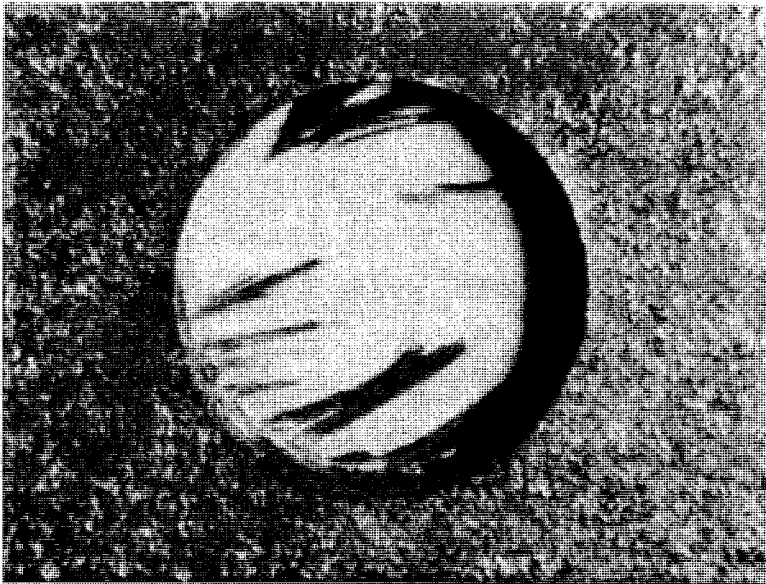


Figure 6: Entry face of H1-A-1 drilled at .0178 m/min feed with HSS bit. Note that the major damage seen is from the exit face. {X 8.5}

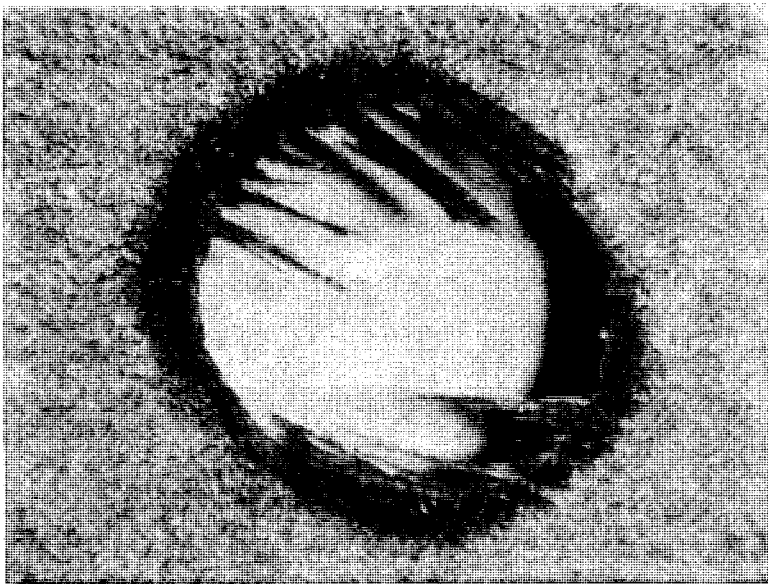


Figure 7: Exit face of H1-A-1 drilled at .0178 m/min feed with HSS bit. {X 8.5}

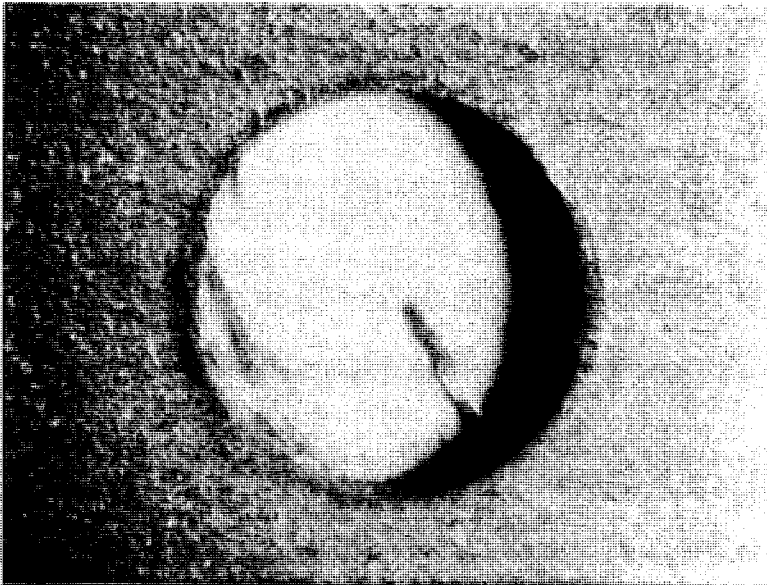


Figure 8: Entry face of H2-B-6 drilled at .0508 m/min feed with HSS bit. Note that major damage seen is from the exit face. {X 8.5}

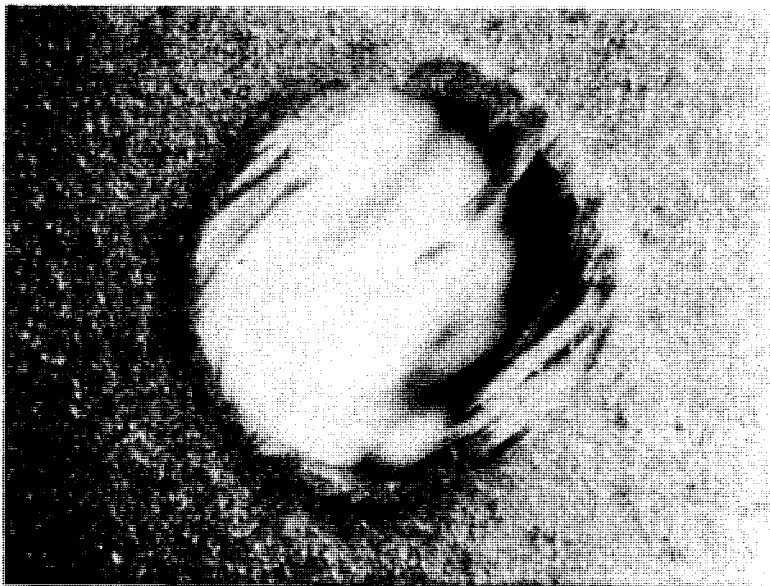


Figure 9: Exit face of H2-B-6 drilled at .0508 m/min feed with HSS bit. {X 8.5}

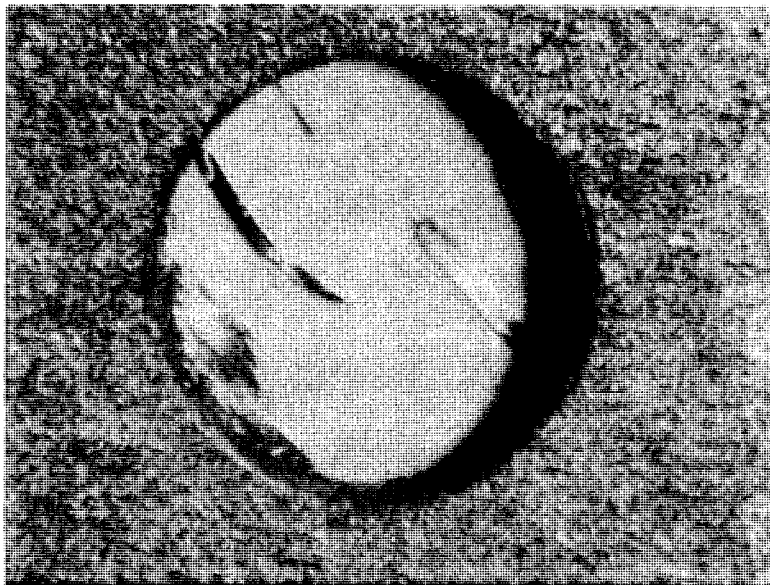


Figure 10: Entry face of H3-C-9 drilled at .153 m/min feed with HSS bit. Note that major damage seen is from the exit face. {X 8.5}

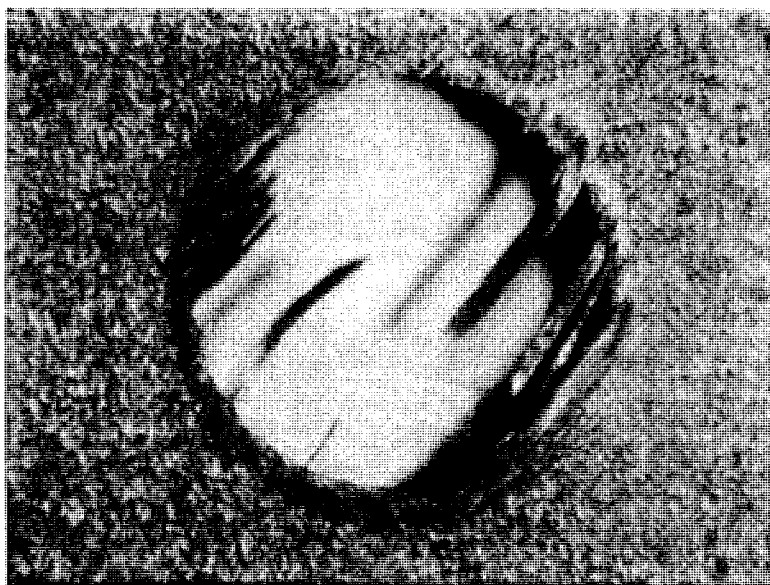


Figure 11: Exit face of H3-C-9 drilled at .153 m/min feed with HSS bit. {X 8.5}

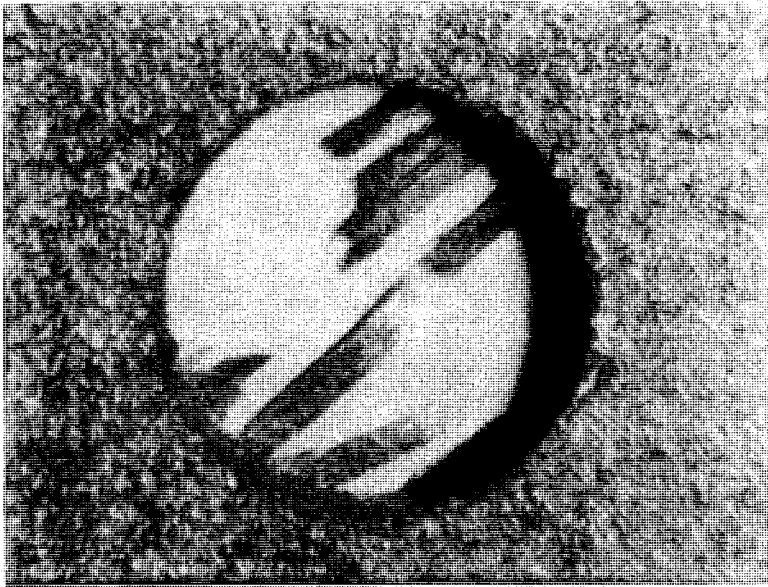


Figure 12: Entry face of H4-D-13 drilled at .457 m/min feed with HSS bit. Note that major damage seen is from the exit face. {X 8.5}

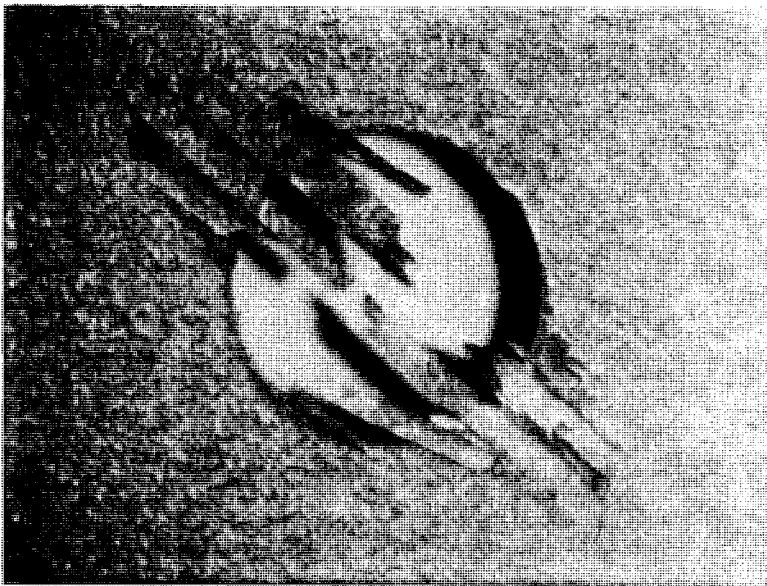


Figure 13: Exit face of H4-D-13 drilled at .457 m/min feed with HSS bit. {X 6.5}

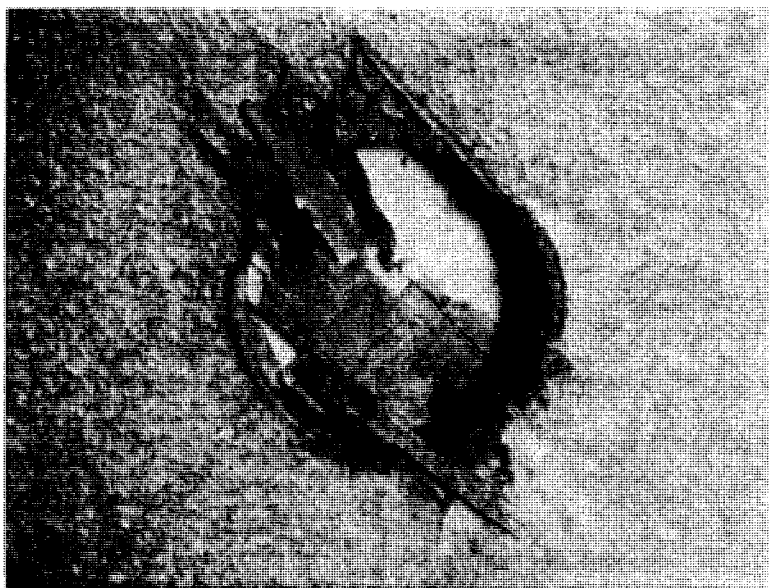


Figure 14: Entry face of H5-E-18 drilled at 1.37 m/min feed with HSS bit. {X 6.5}

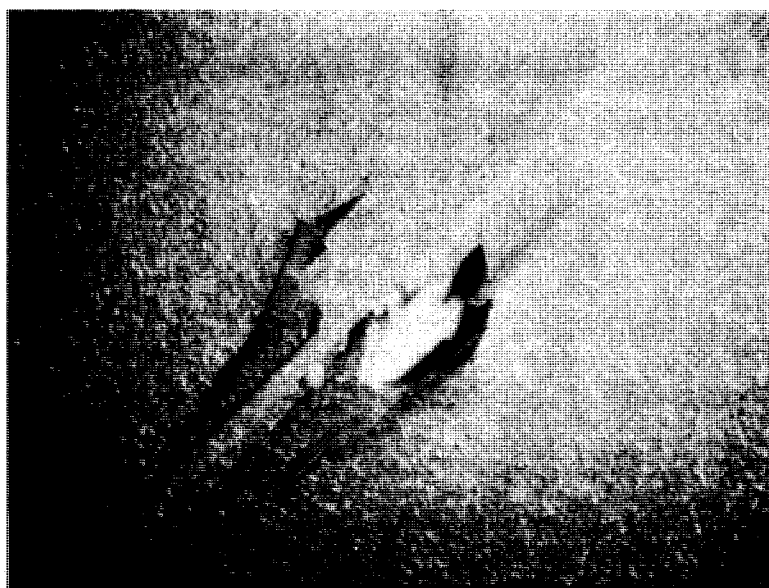


Figure 15: Exit face of H5-E-18 drilled at 1.37 m/min feed with HSS bit. {X 4}



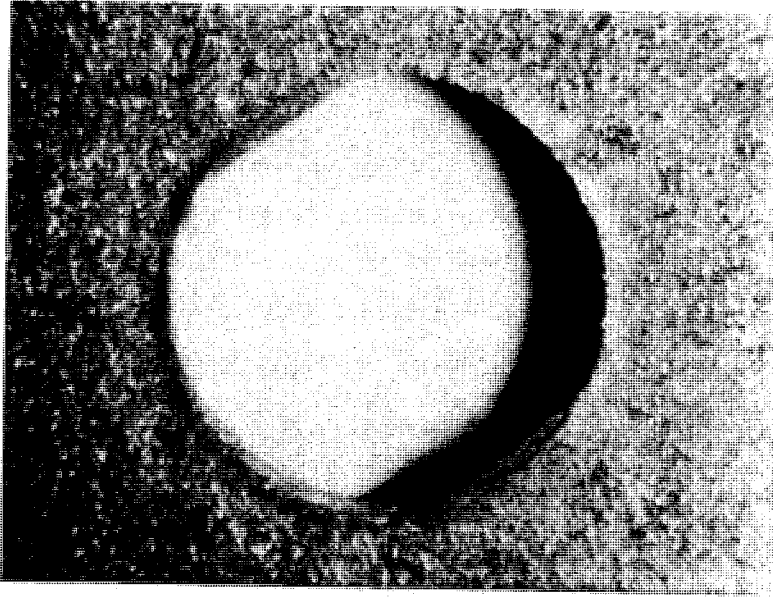


Figure 16: Exit face of C1-A-19 drilled at .0178 m/min feed with carbide bit. {X 9}

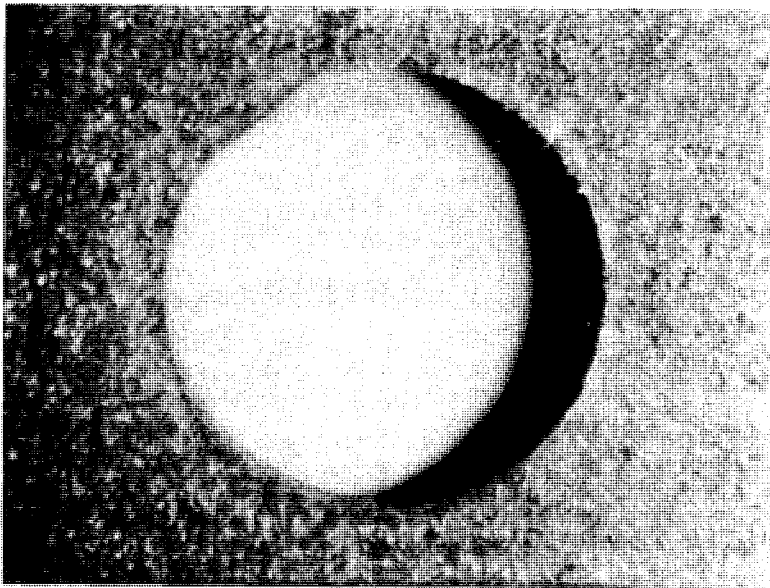


Figure 17: Exit face of C1-B-20 drilled at .0508 m/min feed with carbide bit. {X 9}

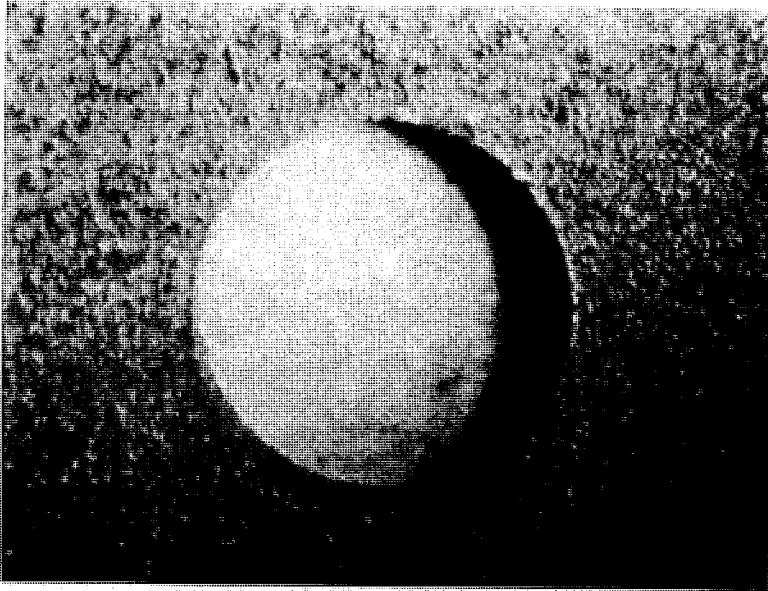


Figure 18: Exit face of C1-C-21 drilled at .153 m/min feed with carbide bit. {X 8}

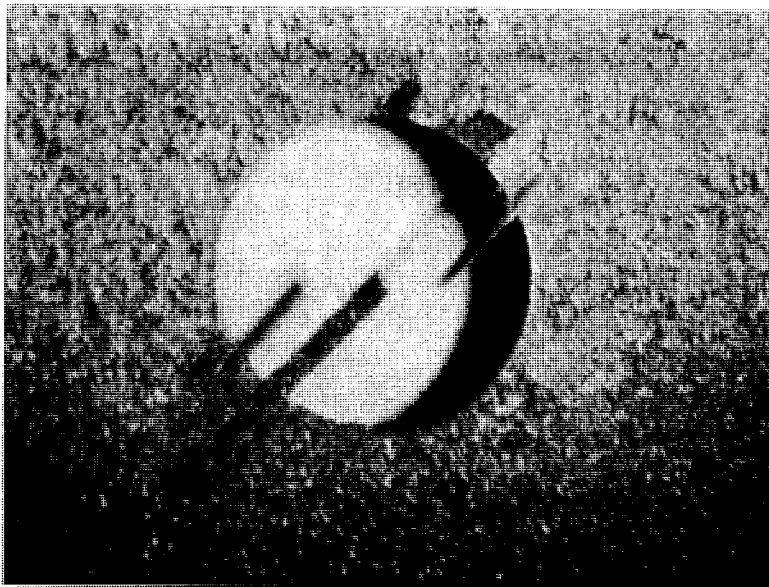


Figure 19: Exit face of C1-D-22 drilled at .457 m/min feed with carbide bit. {X 6.5}

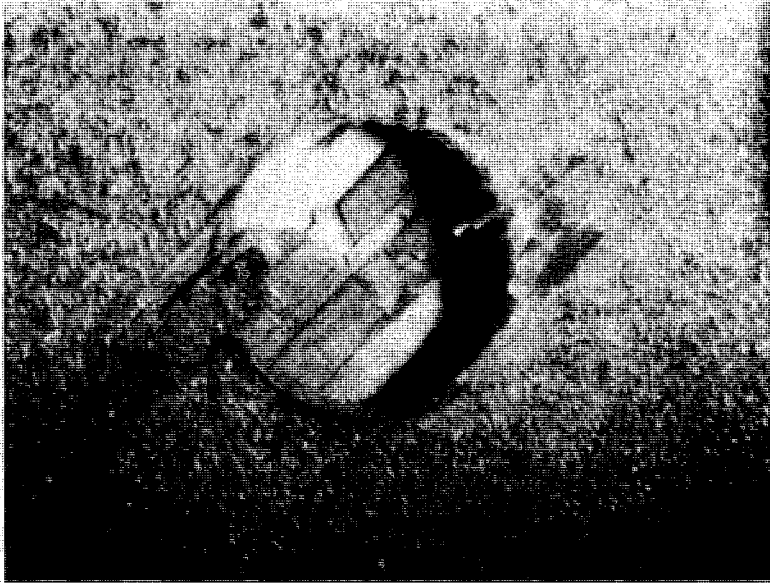


Figure 20: Entry face of C1-E-23 drilled at 1.37 m/min feed with carbide bit. {X 6}

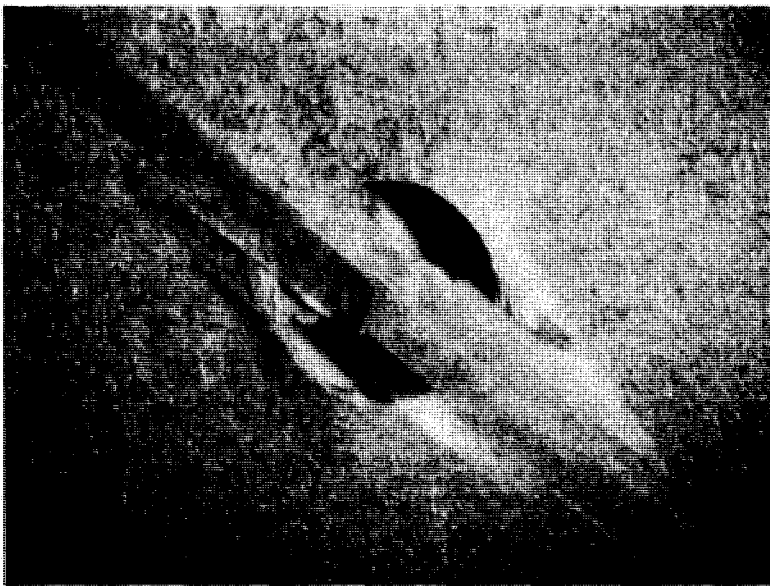


Figure 21: Exit face of C1-E-23 drilled at 1.37 m/min feed with carbide bit. {X 4.5}



Figure 22: Edge view of cutting edge on new HSS drill bit. {X 25}

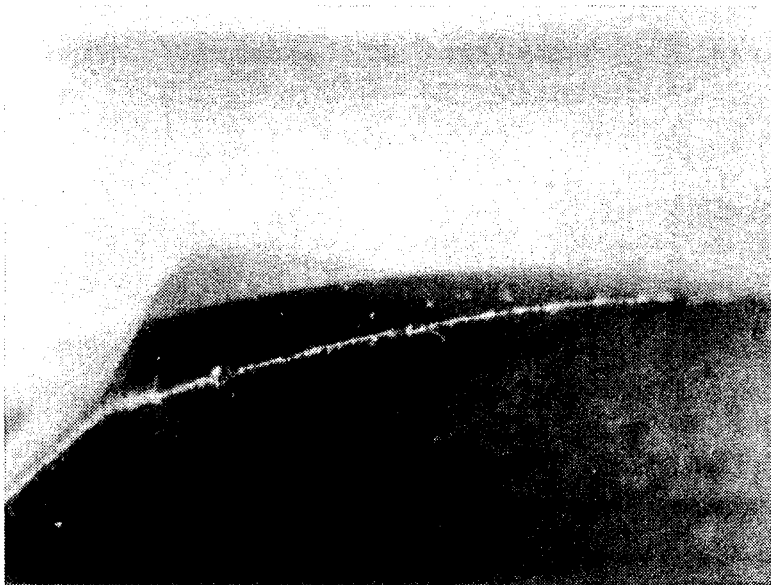


Figure 23: Edge view of cutting edge on used HSS bit. Note minor pitting when compared with Fig. 22. {X 25}

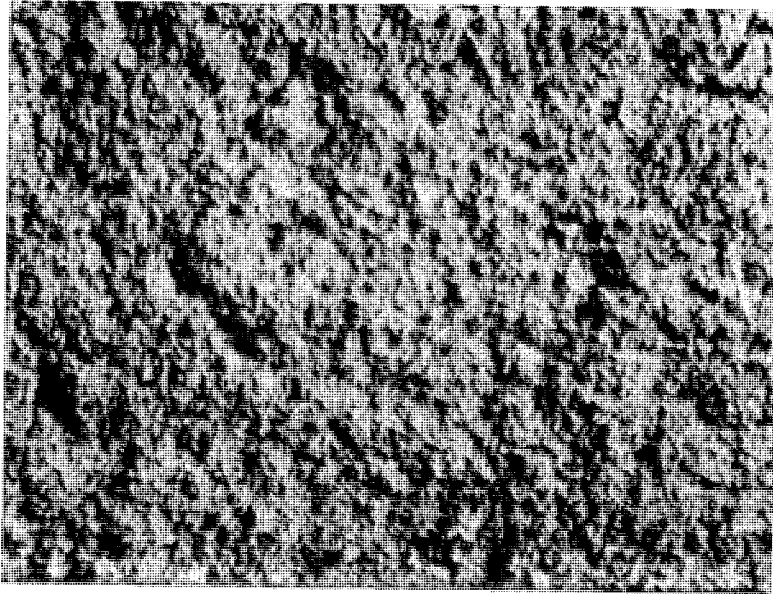


Figure 24: Lowest feed (.0178 m/min) chips which are a fine powder. {X 10}



Figure 25: Highest feed (1.37 m/min) chips which range from 1 ~ 4 mm in size. {X 10}

Table 3: Damage comparison between HSS and carbide bits based upon length of damage away from hole.

Sample		Feed Rate (m/min)	Length of Damage Away From Hole (mm)	
HSS	Carbide		HSS	Carbide
H1-A-1	C1-A-19	.0178	1	0
H2-B-6	C1-B-20	.0508	0.7	0
H3-C-9	C1-C-21	.153	0.7	0
H4-D-13	C1-E-23	.457	4	1
H5-E-18	C1-E-23	1.37	11	8.2

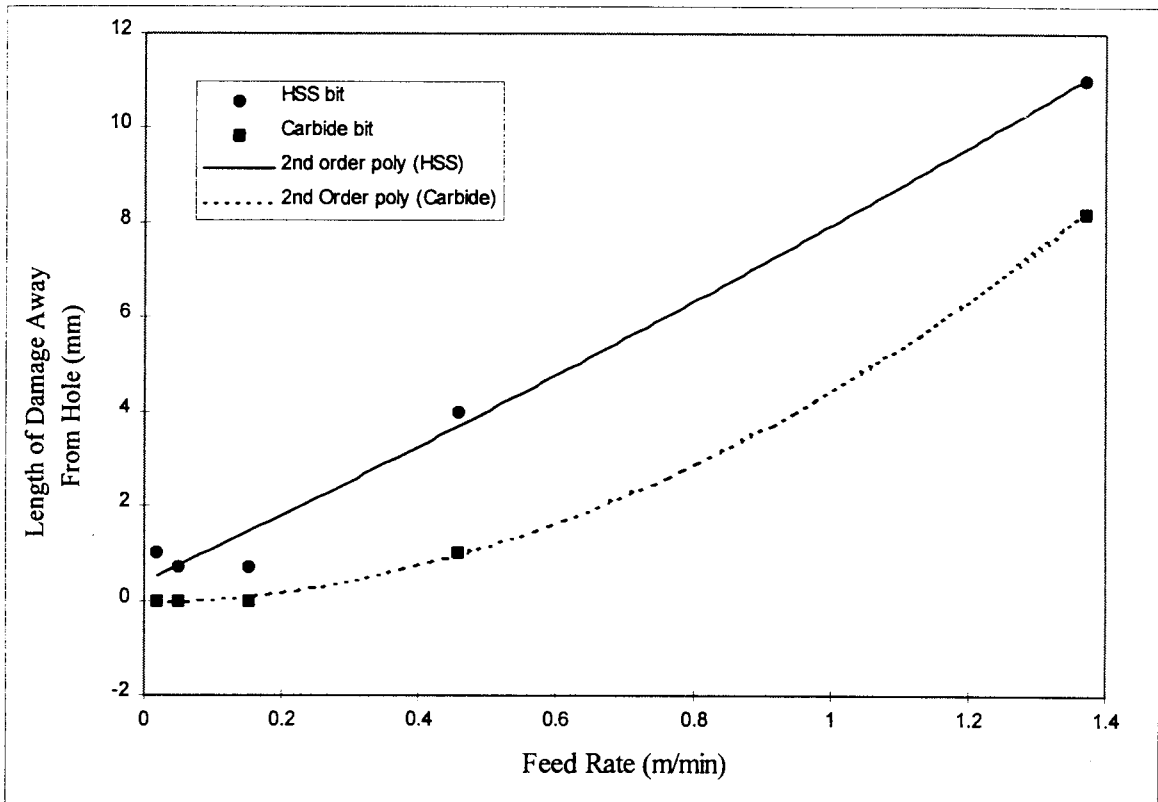


Figure 26: Damage comparison between HSS and carbide bits based upon the length of damage away from hole.

Table 4: Damage comparison between HSS and carbide bits based upon the percentage of hole area blocked by protruding fibers.

Sample		Feed Rate (m/min)	Percentage of Hole Area Blocked By Protruding Fibers	
HSS	Carbide		HSS	Carbide
H1-A-1	C1-A-19	.0178	26	3
H2-B-6	C1-B-20	.0508	13	1.5
H3-C-9	C1-C-21	.153	22	0
H4-D-13	C1-E-23	.457	32	8.6
H5-E-18	C1-E-23	1.37	82	74

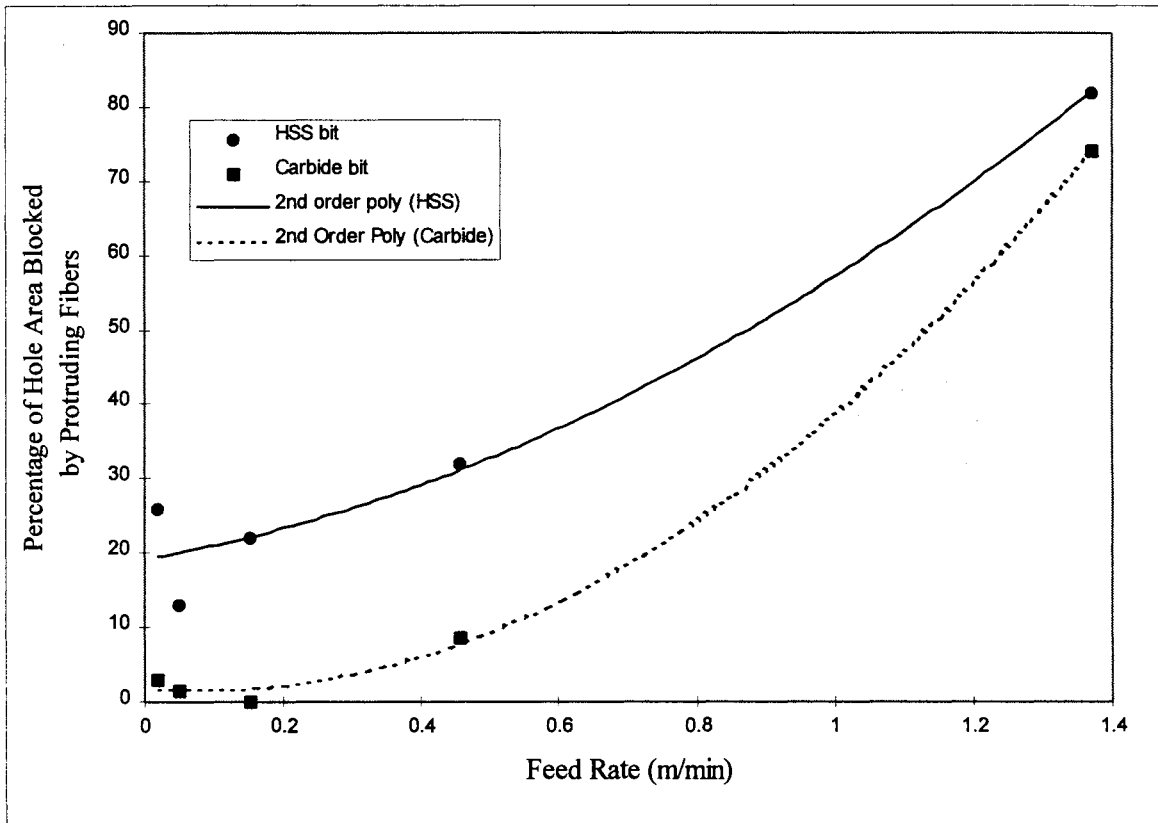


Figure 27: Damage comparison between HSS and carbide bits based upon percentage of hole area blocked by protruding fibers.

### Strength Testing

A number of tensile tests were performed to characterize the material's strength.

A total of 32 specimens were broken and a summary of all tests is shown in Appendix A.

The mean strength  $S_m$  of all the tensile tests is 30.0 KN (6734 lb) with a standard deviation of  $\pm 1\%$ . During a typical tensile test, the material fractured at a strain of 1.58 mm which is 1.04% of the gauge length.

To see if the damage around the holes had any bearing on tensile strength, one specimen at each of the five feed rates was tensile tested at a head rate of .051 mm/s (.002 in/s). The results are shown in Table 5 and Fig. 28.

Table 5: Tensile strengths of specimens drilled with different feed rates. Tensile testing performed at a head rate of .0508 mm/s or a strain rate of  $8.5 \times 10^{-3}$  mm/mm/s.

Sample	Feed Rate m/min (in/min)	Tensile Strength KN (lb)	Maximum Stress KPa (ksi)
H1-A-2	.0178 (0.7)	29.8 (6700)	319.6 (71.9)
H2-B-7	.0508 (2)	29.8 (6704)	319.8 (71.9)
H6-C-25	.153 (6)	29.9 (6719)	320.5 (72.1)
H4-D-13	.457 (18)	29.9 (6730)	321.1 (72.2)
H5-E-17	1.37 (54)	29.6 (6662)	317.8 (71.5)



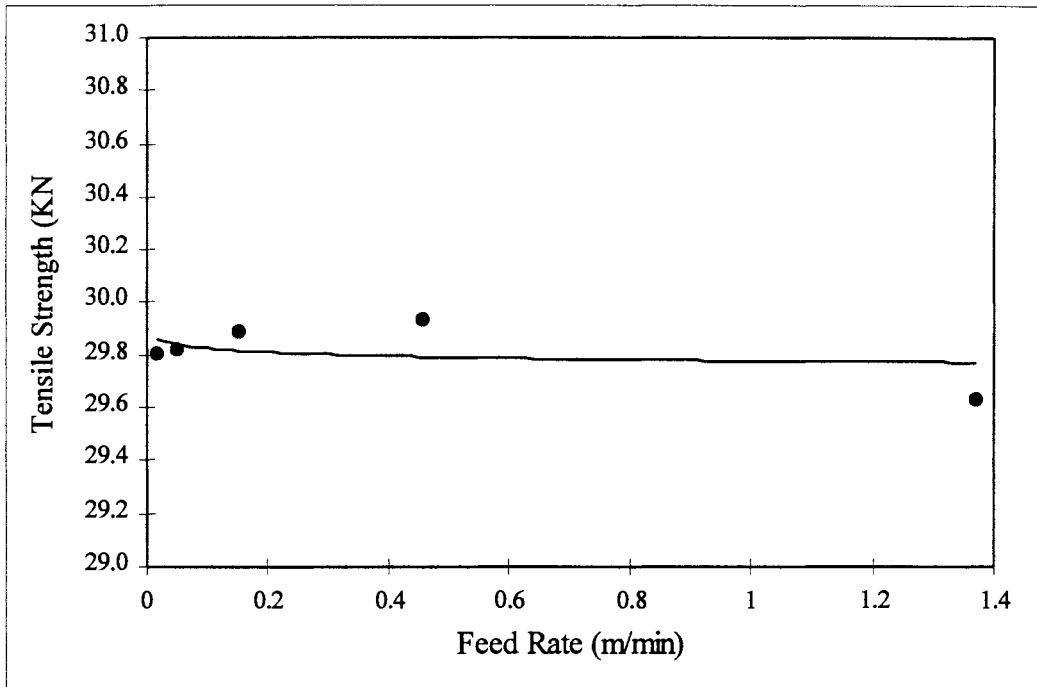


Figure 28: Effect of feed rate on tensile strength. All tensile tests performed at .051 mm/s head rate.

To predict the general trend of head rate on tensile test strength a number of samples with different feed rates were tested. Table 6 and Fig. 29 display the results. Although not shown on Fig. 29, a tensile test was also performed at 20.3 mm/s to determine the strain rate sensitivity of the material. The resulting strength of the 20.3 mm/s test is 30 KN.

An accidental residual strength test occurred during fatigue testing of specimen H3-C-28. The resulting residual strength of 35.7 KN was 19% higher than the tensile strength. To further investigate this interesting effect, residual strength tests were performed on a number of specimens which had experienced a previous fatigue history. The residual strength testing results are shown in Table 7 and Fig. 30.

Table 6: Tensile test summary

Sample	Feed Rate m/min (in/min)	Head Rate mm/s (in/s)	Tensile Strength KN (lb)	Maximum Stress MPa (ksi)
H6-C-24	.153 (6)	.013 (.0005)	29.9 (6722)	497 (72.0)
H6-C-27	.153 (6)	.004 (.00015)	29.7 (6685)	494 (71.7)
H1-A-2	.0178 (0.7)	.051 (.002)	29.8 (6700)	495 (71.9)
H2-B-7	.0508 (2)	.051 (.002)	29.8 (6704)	496 (71.9)
H4-D-13	.457 (18)	.051 (.002)	29.9 (6730)	498 (72.2)
H5-E-17	1.37 (54)	.051 (.002)	29.6 (6662)	493 (71.5)
H6-C-25	.153 (6)	.051 (.002)	29.9 (6719)	496.8 (72.1)
H6-C-26	.153 (6)	.13 (.005)	30.5 (6848)	506.4 (73.4)
H3-C-9	.153 (6)	.203 (.008)	30.6 (6870)	508 (73.7)
C1-A-41	.0178 (0.7)	.25 (.01)	29.8 (6700)	495 (71.9)

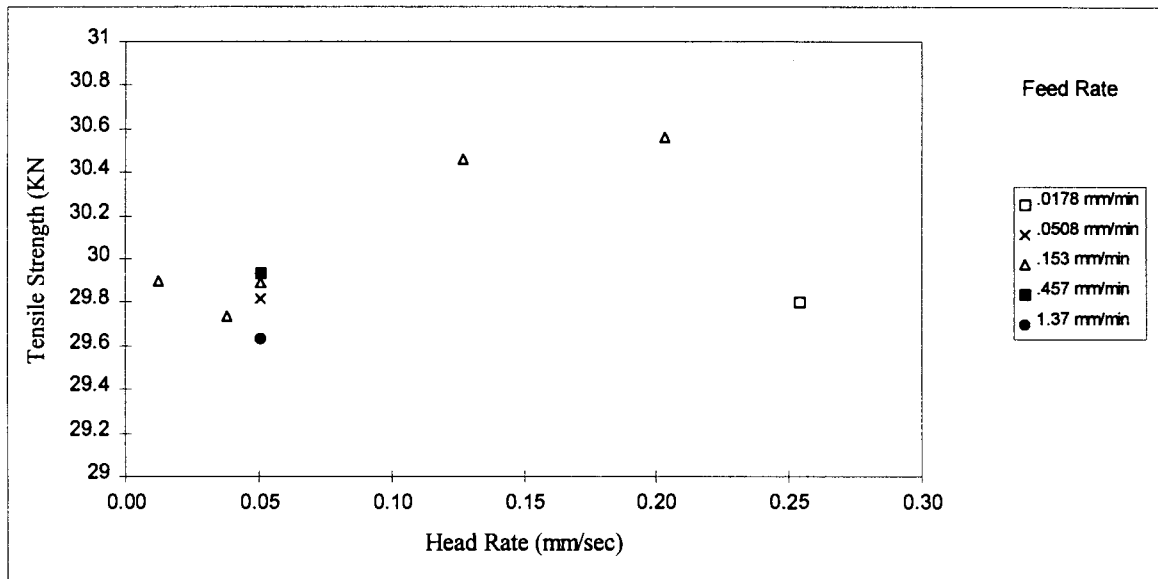


Figure 29: Tensile test results at various head rates and feed rates.

Table 7: Residual strength tests at constant feed rate of .153 m/min and a constant head rate of .051 mm/s which corresponds to a strain rate of  $3.33 \times 10^{-4}$  mm/mm/s.

Sample	Cycles @ 9 Hz		Cyclic Stress (MPa)			Residual Strength	
	N	Load Level	Max	Mean	Min	Load (KN)	Stress (MPa)
H6-C-25	~	1 $S_m$	~	~	~	29.9	497
H7-C-31	150	0.93 $S_m$	464	277	95	30.7	510
H7-C-30	1,100	0.93 $S_m$	464	277	95	32.7	544
C1-C-21	10,005	0.93 $S_m$	464	277	95	32.7	544
H8-C-32	10,008	0.93 $S_m$	464	277	95	33.2	552
H3-C-8	199,596	0.93 $S_m$	464	277	95	35.7	593
H8-C-35	380,006	0.93 $S_m$	464	277	95	33.7	560
H7-C-29	1,100,000	0.93 $S_m$	464	277	95	36.1	600
H3-C-10	1,150,855	0.93 $S_m$	464	277	95	37.2	619

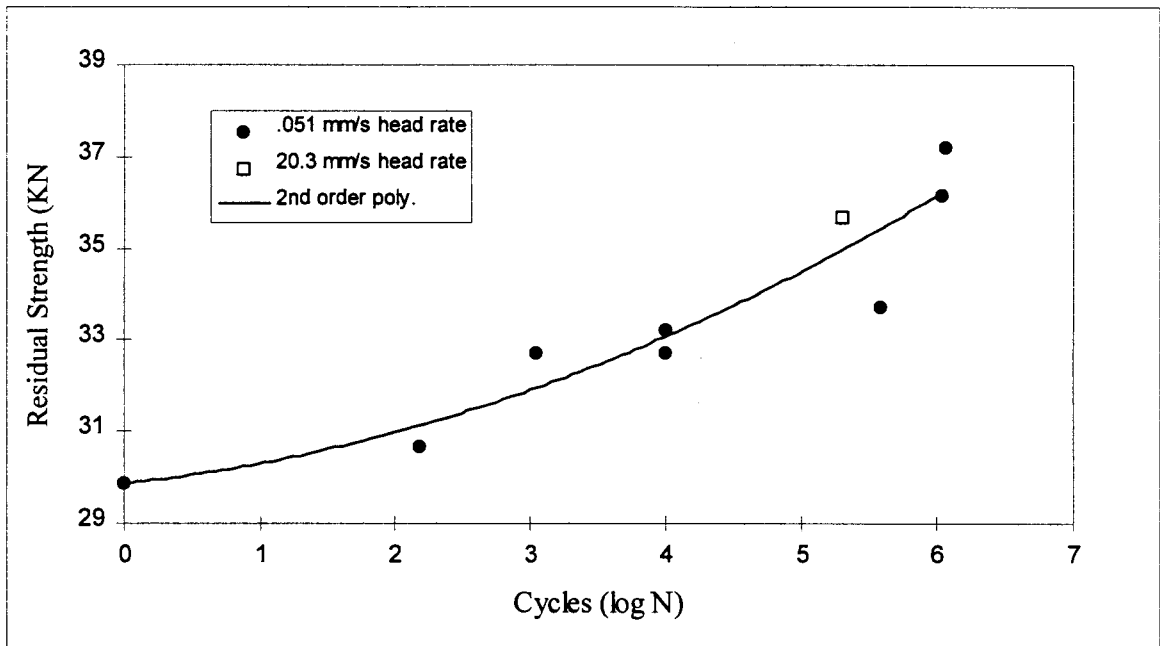


Figure 30: Residual strength testing at a constant feed rate of .153 m/min and a constant head rate of .051 mm/s which corresponds to a strain rate of  $3.33 \times 10^{-4}$  mm/mm/s.

Each of the points from Fig. 30 were used to determine the percent increase in residual strength. Fig. 31 is a graphic portrayal of the increase in residual strength.

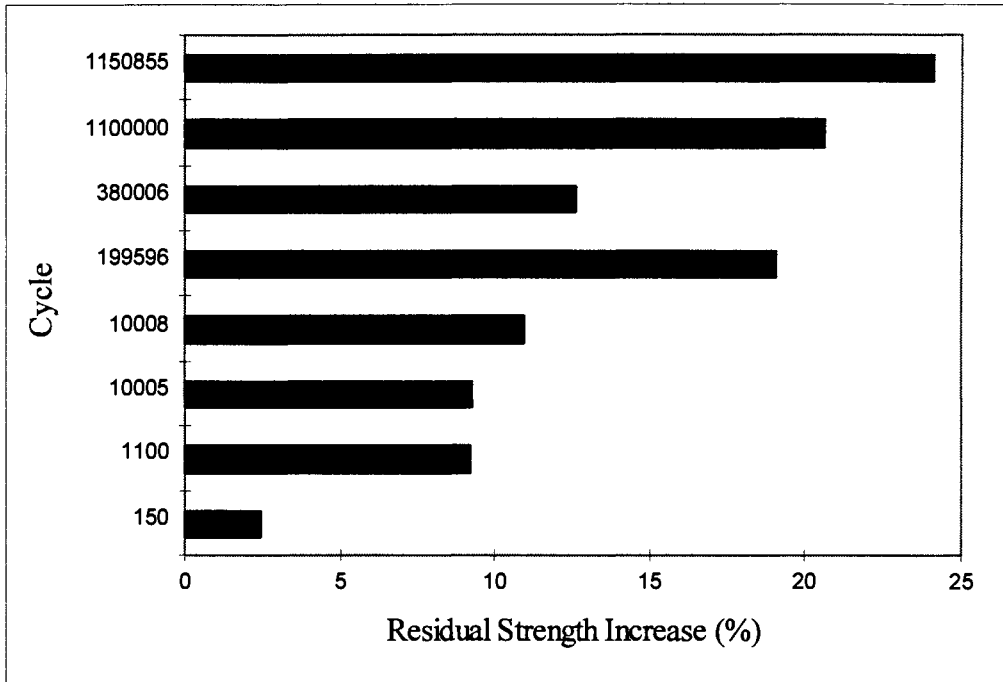


Figure 31: Percent increase in residual strength.

The increase in residual strength appears uniform except for the 199,596 cycle sample (specimen H3-C-8). The only difference between H3-C-8 and the other specimens was the head rate. Further tests were performed to see what effect changing the head rate had on the residual strength. These tests led to Table 8 and Fig. 32 which shows the effect of head rate on residual strength. Note that sample H7-C-28 with a head rate of 20.3 mm/s was used in place of a sample at 13.5 mm/s to. Fig. 33 graphically compares the residual strength at different head rates.

Table 8: Data for effect of head rate on residual strength.

Sample	Feed Rate m/min (in/min)	Head Rate mm/s (in/s)	Cycles N	Residual Strength KN (lb)
H6-C-24	.153 (6)	.013 (.0005)	0	29.9 (6722)
H7-C-28	.153 (6)	20.3 (0.8)	0	30.0 (6739)
H9-C-36	.153 (6)	.013 (.0005)	10,005	32.2 (7247)
H9-C-37	.153 (6)	13.5 (.53)	10,007	32.9 (7392)
H9-C-39	.153 (6)	.013 (.0005)	290,006	33.9 (7621)
H9-C-38	.153 (6)	13.5 (.53)	290,005	35.6 (8005)

Note: All cycles performed at 9 Hz with a load level of  $0.93 S_m$ .

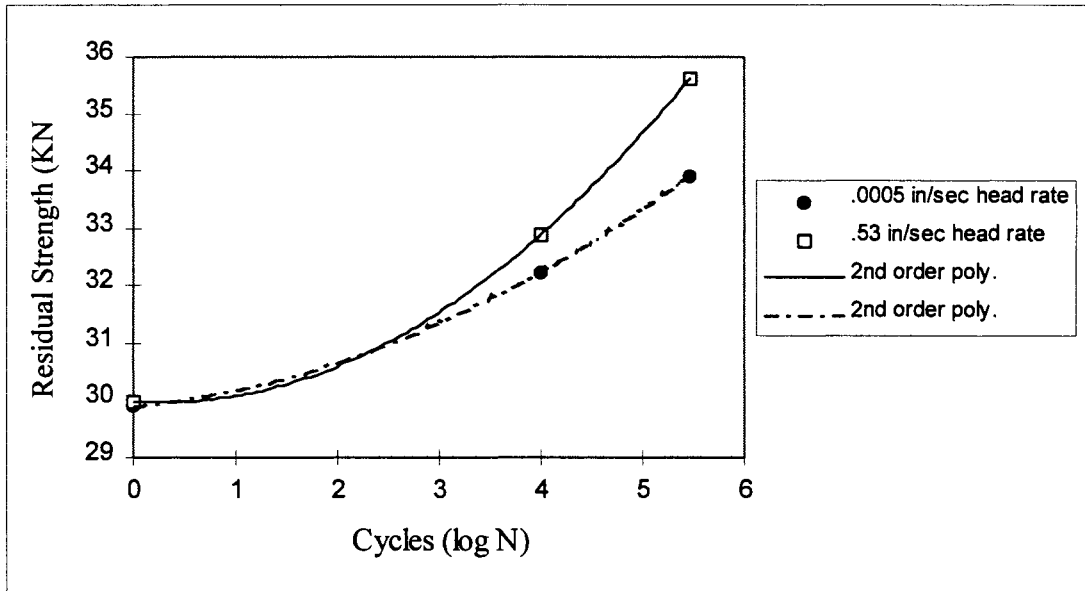


Figure 32: Effect of head rate on residual strength.

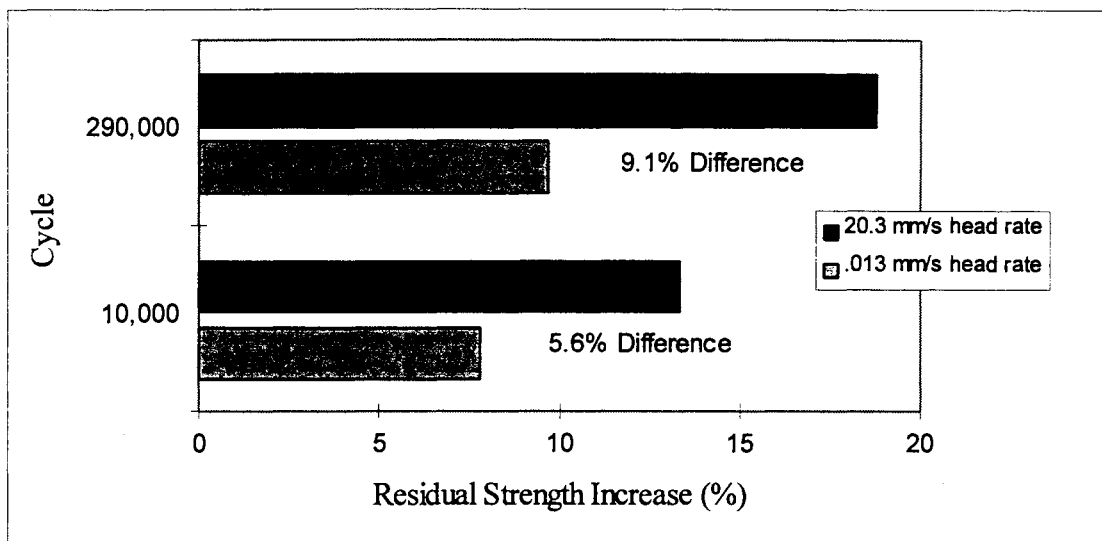


Figure 33: Comparison of residual strength increase at different head rates.

To see what effect the cyclic load level has on residual strength, three samples were strength tested after receiving 10,000 cycles at different load levels. Load levels of 70, 80, and 93 percent of the material's mean strength ( $S_m$ ) were chosen. Table 9 and Fig. 34 reveals the testing results.

Table 9: Effect of cyclic load level on residual strength.

Sample	Cycles @ 9 Hz		Cyclic Stress (MPa)			Residual Strength	
	N	Load Level	Max	Mean	Min	Load (KN)	Stress (MPa)
H8-C-32	10,008	93 %	464	277	95.0	33.2	552
H8-C-33	10,006	81 %	402	240	82.2	32.6	542
H8-C-34	10,008	70 %	352	209	69.9	30.9	514

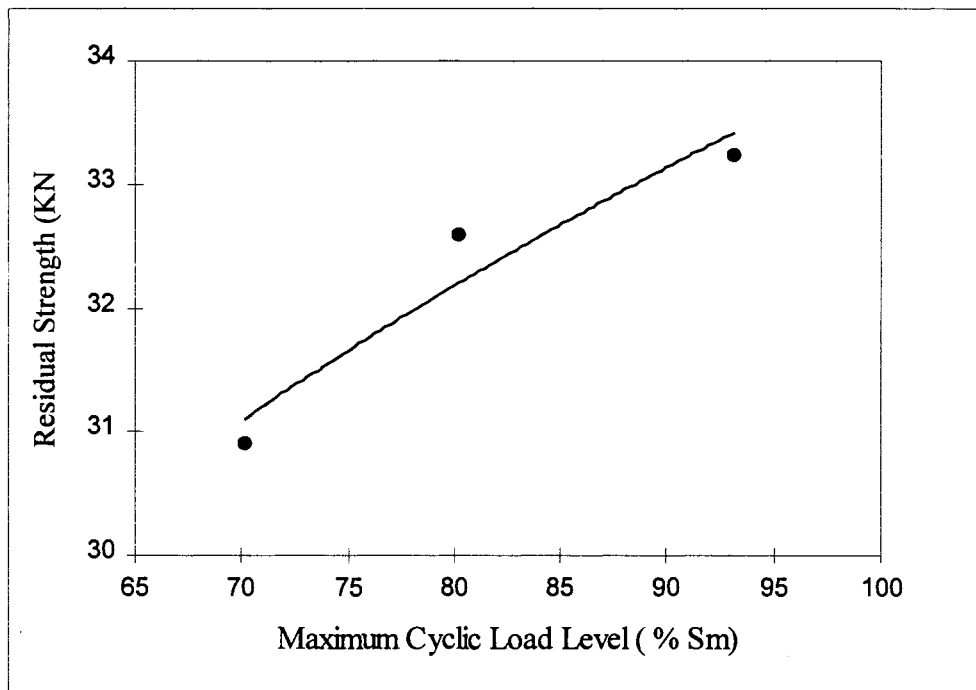


Figure 34: Effect of cyclic load level on residual strength.

Further testing was also performed to see how feed rate effected the residual strength. Five specimens each at a different feed rate were fatigue tested at  $0.93 S_m$  cyclic load level for 10,000 cycles. Combining the resulting residual strength with tensile tests resulted in Table 10 and Fig. 35.

Table 10: Residual strength data at various feed rates. Cyclic testing performed at 0.93  $S_m$  loading at a frequency of 9 Hz.

Sample	Feed Rate m/min (in/min)	Head Rate mm/s (in/s)	Cycles N	Residual Strength KN (lb)
H2-B-7	.0508 (2)	.051 (.002)	0	29.8 (6704)
H6-C-25	.153 (6)	.051 (.002)	0	29.9 (6719)
H4-D-13	.457 (18)	.051 (.002)	0	29.9 (6730)
H5-E-17	1.37 (54)	.051 (.002)	0	29.6 (6662)
H1-B-5	.0508 (2)	.051 (.002)	10,007	32.6 (7331)
H8-C-32	.457 (18)	.051 (.002)	10,008	33.2 (7472)
H4-D-12	.457 (18)	.051 (.002)	10,010	32 (7200)
H5-E-15	1.37 (54)	.051 (.002)	10,010	32.9 (7404)

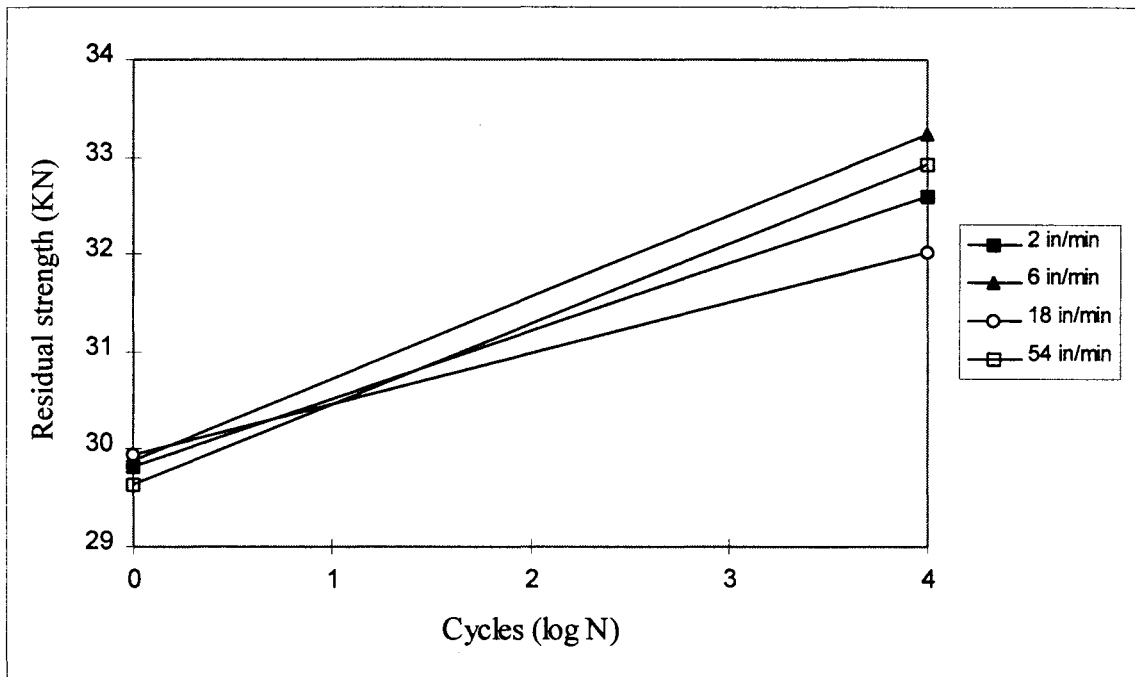


Figure 35: Effect of feed rate on residual strength.



During a 1 million cycle test, a temperature increase was felt by hand. This temperature rise, which occurred during testing, was then documented. Fig. 36 presents the temperature profile for a typical 10,000 cycle test, while Fig. 37 shows the profile for a longer 400,000 cycle test. Both profiles were obtained at  $0.93 S_m$  load level using a frequency of 9 Hz (Note that one hour at 9 Hz corresponds to 32,400 cycles).

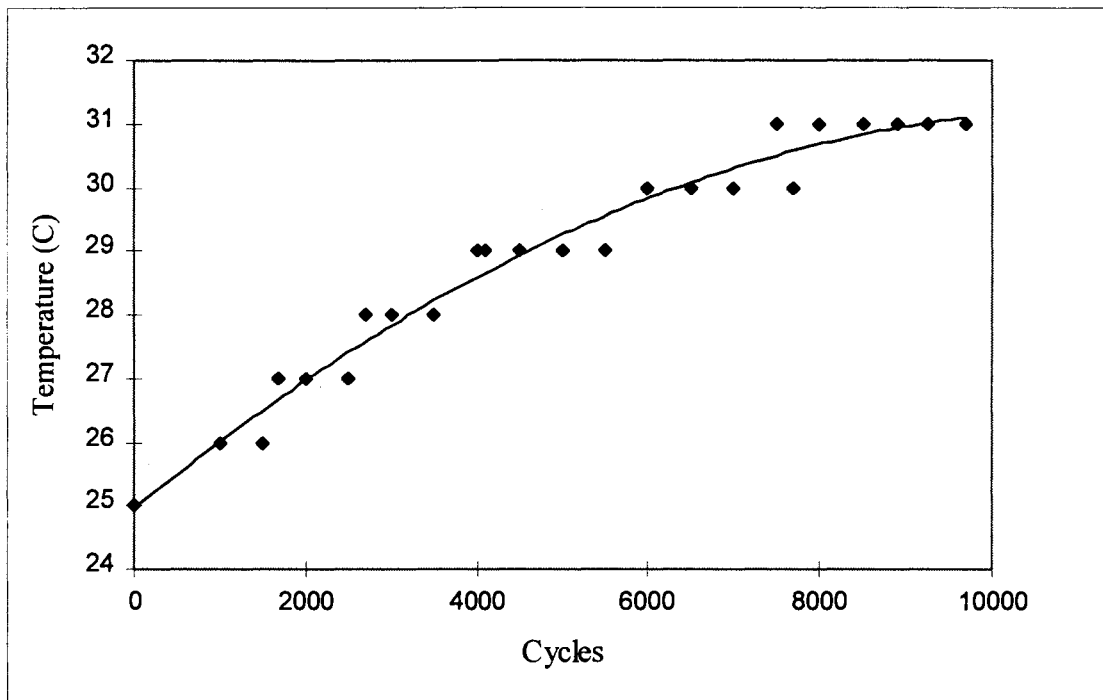


Figure 36: Temperature Profile for 10,000 cycles at 9 Hz. Data taken from specimens H9-C-36 and H9-C-37.

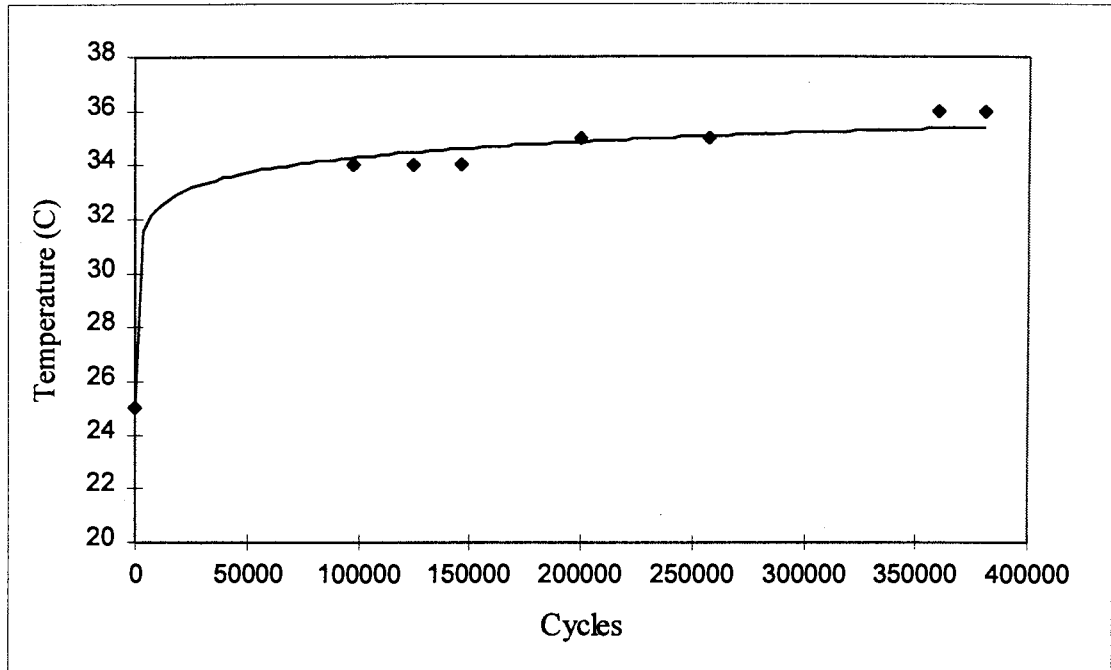


Figure 37: Temperature Profile of 380,000 cycles at 9 Hz (93% load level). Data taken from specimen H8-C-35.

Several pictures were taken through a zoom microscope to document specimen fracture. Figs. 38 and 39 contrast the different fractures at the slowest and fastest head rates. The next figures (Figs. 40 and 41) show the fracture surface of specimens which experienced the highest number of cycles before being residual strength tested. Fig. 42 shows the brooming effect which occurred during high cycle testing. The split between the layers in Fig. 42 is typical of all tests which received 500,000 cycles or more.

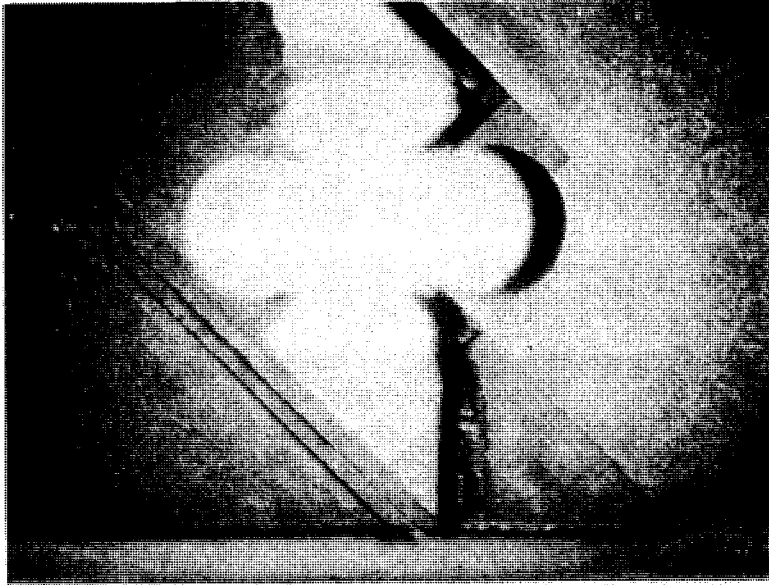


Figure 38: H6-C-27 tensile tested at .004 mm/s head rate (29.7 KN strength). Note uniform and even fracture surface except for 45° ply which did not fracture {X 3.5}



Figure 39: H7-C-28 tensile tested at 20.3 mm/s head rate (30 KN strength). Note uniform and even fracture surface except for 45° ply which did not fracture {X 3.5}

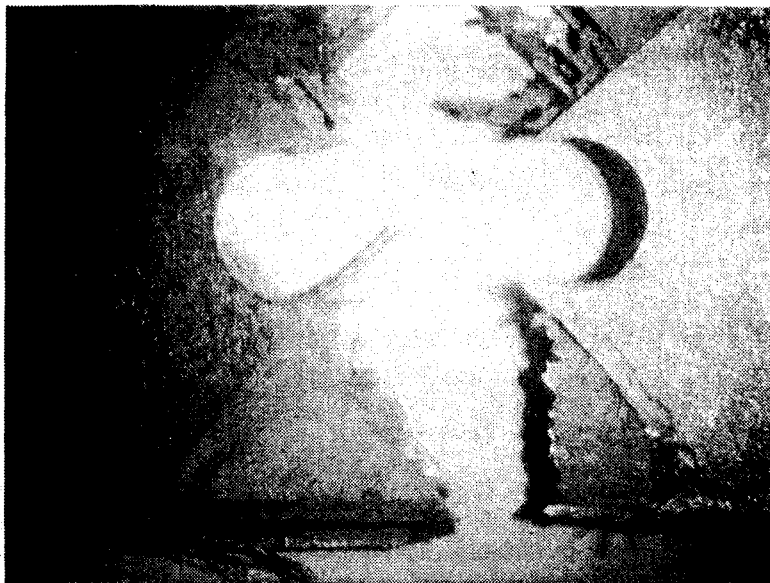


Figure 40: H3-C-10 fatigued at 27.9 KN (93% initial tensile strength) for 1,150,855 cycles. Residual strength was 32.2 KN. View is looking down on bit entry. Note rough and uneven fracture surface. {X 3.5}



Figure 41: H7-C-29 fatigued at 27.9 KN (93% initial tensile strength) for 1,100,000 cycles. Residual strength was 36.1 KN. View is looking down on bit entry. Note rough and uneven fracture surface {X 3.5}

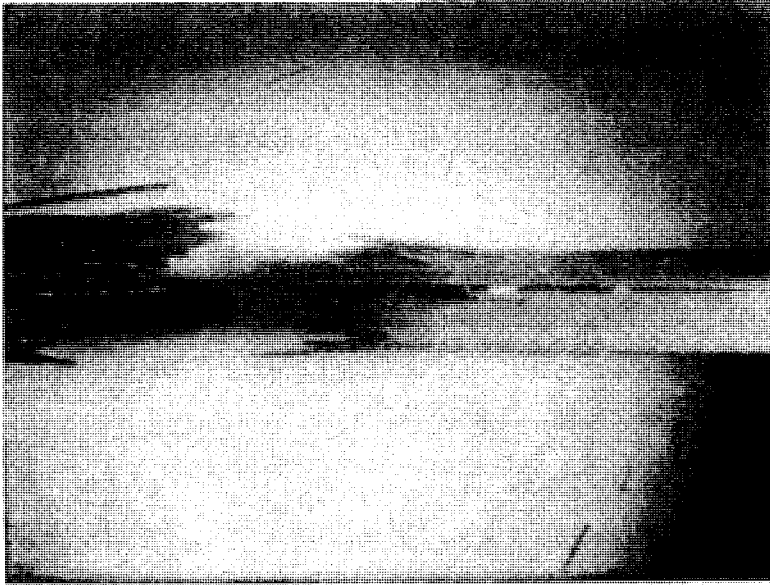


Figure 42: Side view of H3-C-10. Note brooming effect at left and ply separation in middle of thickness at right. {X 4}

## Scanning Electron Microscopy

A scanning electron microscope was used to get a more detailed look at the fractured and machined specimen surfaces. All of the SEM pictures are one of three views, as shown specifically in Fig. 43.

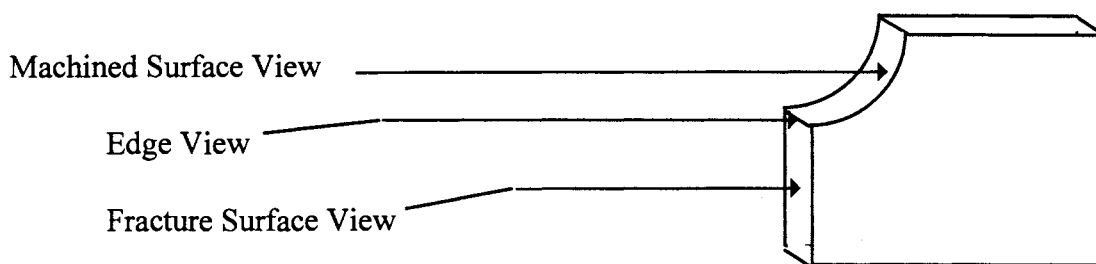


Figure 43: SEM view description.

Where possible, corresponding views and magnifications are presented on the same page to allow for ease of comparison. Also, the pictures taken were representative of the entire fracture surface. When studying SEM pictures note the following:

1. A larger dark fracture surface region in Fig. 44 than the region seen in Fig. 45.
2. Bumps on 90° fibers in upper portion of Fig. 46.
3. Brittle fracture surface at ends of fibers shown in Fig. 48
4. Lack of ply separations in Fig. 49.
5. Ply separations around 45° plies at left of picture in Fig. 50, while no separations are seen in Fig. 54.

6. Larger dark gaps around 45° plies in Fig 50 then seen in Figs. 51 and 54.
7. Ply separations around 45° plies in Fig. 52, while separations are not seen in Fig 53.
8. Machined area in Fig. 53 is not as well defined and appears smeared when compared with similar machine area shown in Fig 52.

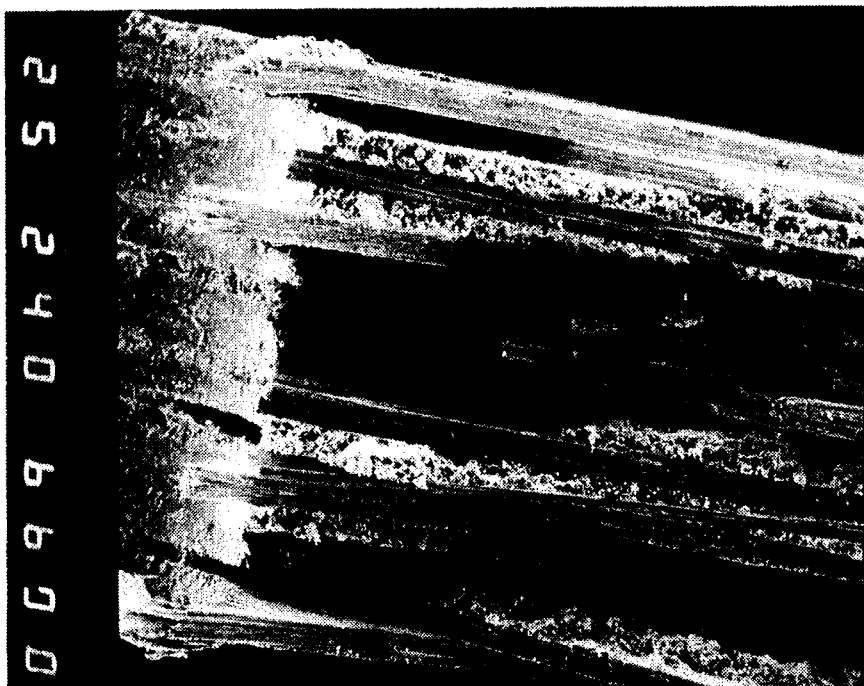


Figure 44: Edge view taken from H3-C-28 which was drilled at .153 m/min feed (bit entry at top of picture). Specimen was tensile tested at 20.3 mm/s head rate which corresponds to head rate during a 9 Hz fatigue test. {X 24}



Figure 45: Edge view taken from H6-C-27 which was drilled at .153 m/min feed (bit entry at bottom of picture). Specimen was tensile tested at slow head rate of .004 mm/s. {X 24}



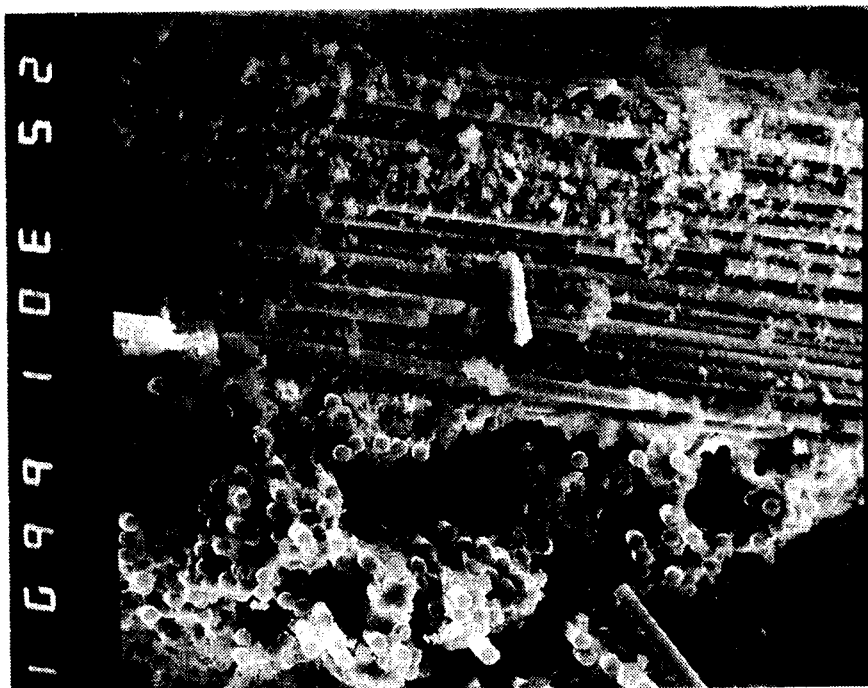


Figure 46: Fracture surface view of H3-C-28. Upper half of picture is 90° fibers while lower half is 0° fibers. Specimen experienced fast strain rate tensile test. {X 300}

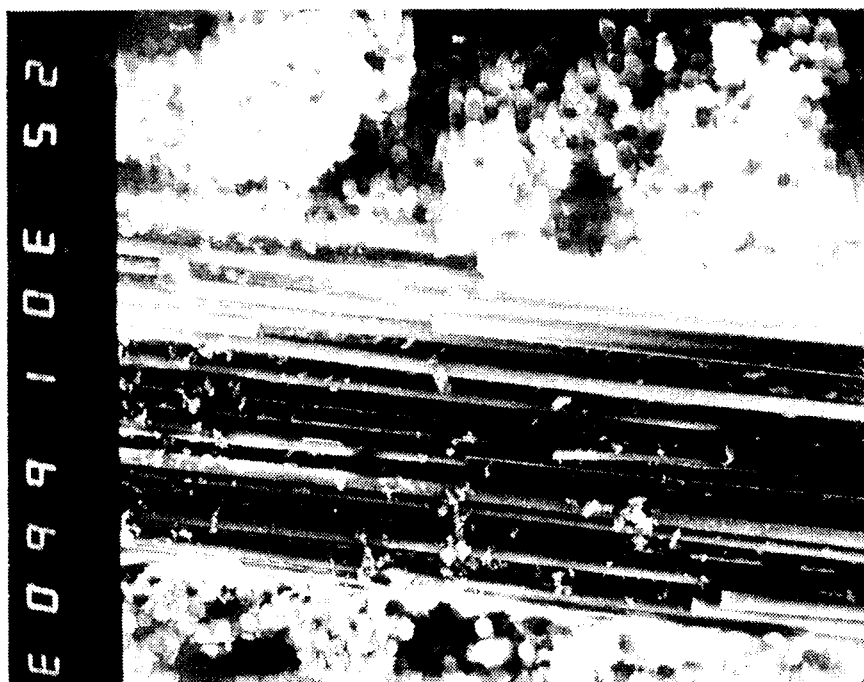


Figure 47: Fracture surface view of H6-C-27. Upper half is 0° fibers while lower portion is 90° fibers. Specimen experienced slow head rate tensile test. {X 300}

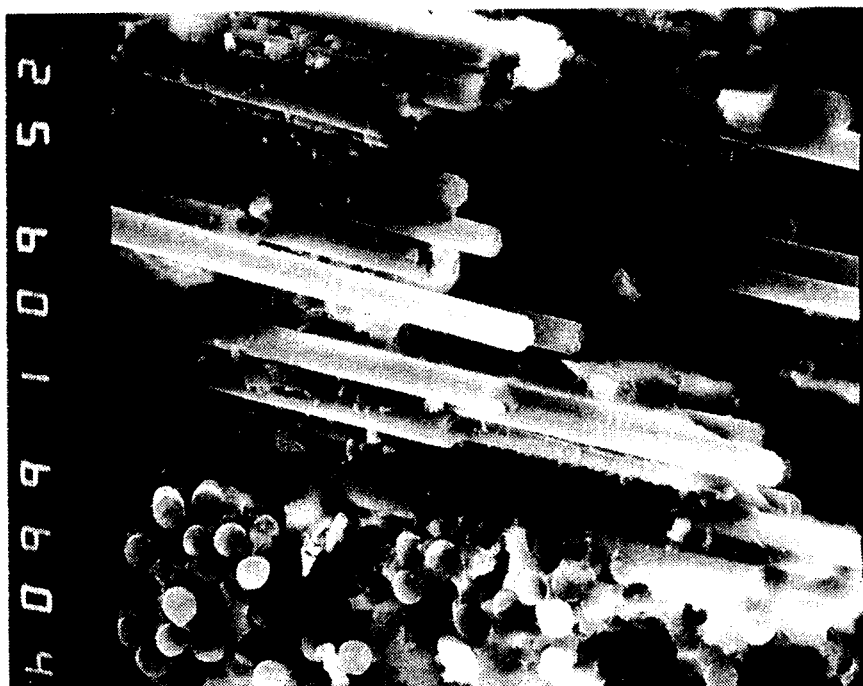


Figure 48: Fiber detail taken from fracture view of specimen H6-C-27. Specimen was tensile tested at slow head rate. {X 600}



Figure 49: Machined surface view of specimen H3-C-28. Specimen drilled at .153 m/min feed (bit entry at top of picture). Specimen experienced fast strain rate tensile test. {X 24}

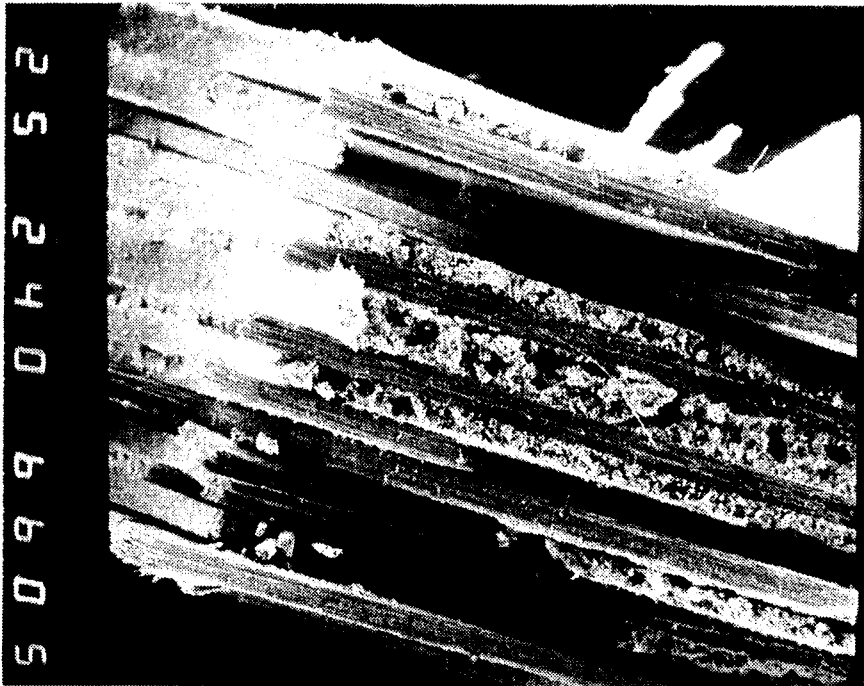


Figure 50: Edge view taken from H7-C-29 which was drilled at .153 m/min feed (bit entry at top of picture). Specimen experienced 1,100,000 cycles at 27.9 KN (93% initial tensile strength). Residual strength was 36.1 KN. {X 24}

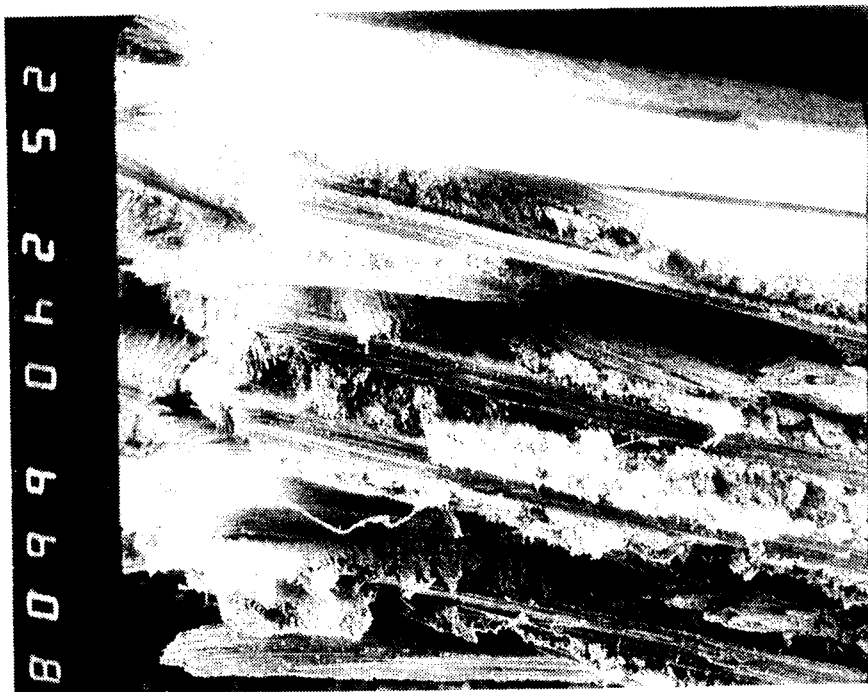


Figure 51: Edge view taken from H5-E-15 which was drilled at 1.37 m/min feed (bit entry at bottom of picture). Specimen experienced 10,010 cycles at 27.9 KN (93% initial tensile strength). Residual strength was 32.9 KN. {X 24}

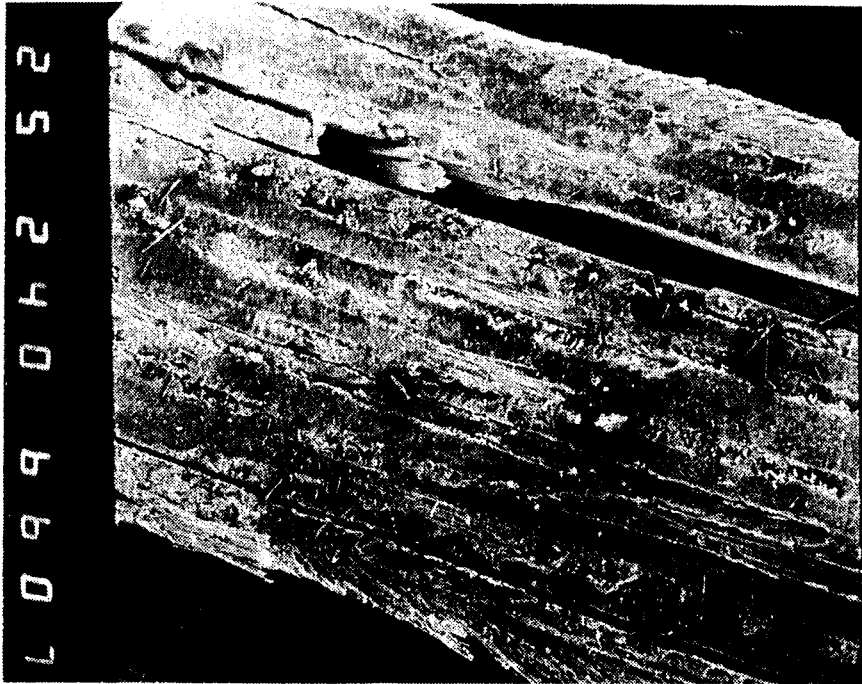


Figure 52: Machine surface detail from H7-C-29 (same sample as Fig. 50). Top bit entry at .153 m/min feed. 1,100,000 cycles at 27.9 KN resulted in a residual strength of 36.1 KN. {X 24}



Figure 53: Machined surface view from H5-E-15 (same sample as Fig. 51). Bottom bit entry at 1.37 m/min feed. 10,010 cycles at 27.9 KN resulted in a 32.9 KN residual strength. {X 24}



Figure 54: Edge view taken from H2-B-7 which was drilled at .0508 m/min feed (bit entry at top of picture). Specimen was tensile tested at .051 mm/s head rate with a strength of 29.8 KN. {X 24}

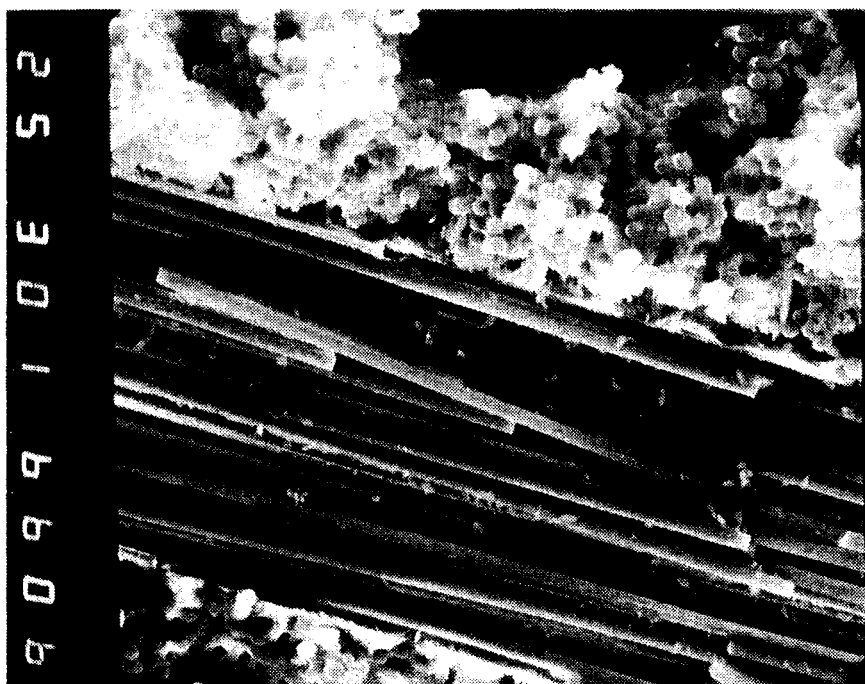


Figure 55: Fracture surface detail of H7-C-29. Upper half is 0° fibers while lower portion is 90° fibers. 1,100,000 cycles at 27.9 KN resulted in a 36.1 KN residual strength. {X 300}

## CHAPTER 5

### DISCUSSION

Tool wear differences between the HSS bit and the carbide bit were initially thought to have been controlled. The carbide bit was not replaced due to superior wear resistance properties, while the HSS bits were replaced frequently in an effort eliminate wear as a parameter. During machining, the edges of the HSS bit did not appear to have any damage even before replacement. However, later microscopic examination showed minor pitting of the cutting edge (see Figs. 22 and 23). Although the amount of tool wear is not believed to be significant enough to affect the damage accumulation, future studies should use a new HSS bit for every hole to fully insure that wear does not affect damage accumulation.

The exit damage produced by the HSS bit was similar at the first three feeds of 0.0178, 0.0508 and 0.153 m/min (see Figs. 6 ~ 11). Damage from the HSS bit at these feeds is characterized by delamination of the outer exit 45° ply around the entire hole. As a result of delamination, the final ply was not cut cleanly by the bit, which left a portion of the final ply protruding into the hole. At the two fastest HSS feed rates of .457 m/min

and 1.37 m/min, the level of damage increased (see Figs. 12 ~ 15, 26 and 27). The increase is due to the speed at which drilling occurs. At these speeds the material is actually being punched rather than drilled. When it is punched, the bit does not cut the final ply, it simply punches through it leaving the entire final 45° ply broken and protruding into the hole. The final ply is also ripped out of the surrounding matrix resulting in a damage zone which extends farther into the material away from the hole but not necessarily through the thickness of the laminate (see Fig 26). Using a HSS bit at a feed of .457 m/min the damage is clearly evident 4 mm away from the hole, while at 1.37 m/min the damage extends 11 mm. Although damage occurred using the HSS bit at all feed rates, this was expected because a backing plate was not used.

The split point carbide bit did not produce the same level of damage as the HSS bit. As previously stated, the reason for the difference is likely related to tool geometry rather than bit material. A split point bit has a reduced web section which in turn requires lower drilling force. With a lower drilling force, less delamination occurs [4]. However, at 1.37 m/min, which was the highest feed, the damage for both the HSS and the carbide bits is similar. This implies that at some feed level the bit geometry advantages are nullified and the same degree of damage is obtained.

From Fig. 28, it is quite clear that although the feed rates produced different amounts of damage, there was not a significant change in tensile strength. Hegde [7] came to the same conclusion for a PPS/glass fiber reinforced composite. Hegde also concluded that head rate effected the tensile strength results. But for a graphite epoxy it appears that the head rate does not have the same effect on the tensile strength (see Fig.

29). This may be due to differences in the viscoelastic behavior of a thermoset and thermoplastic matrix. It is interesting to note that the strain of 1.04% experienced during testing is identical to results obtained by Stinchcomb [30] on a graphite epoxy  $[0^\circ/\pm 45^\circ/90^\circ]_S$  laminate.

Corresponding to previous research on graphite epoxy, the graphite epoxy laminate was found to be fatigue resistant. As many as a million cycles at  $0.93 S_m$  were recorded. Since both graphite and epoxy do not exhibit cyclic plastic deformation the fatigue insensitivity is expected. The strain at fracture also matched closely with previous findings. However, some differences during testing were observed. On a macroscopic scale, longitudinal cracks originating from the hole were not seen. These types of cracks had been observed by both Powers [22] while testing PPS/glass fiber laminate and Shutz [23] in a graphite/epoxy laminate. Another difference was the  $9^\circ\text{C}$  temperature increase which started at the onset of testing. When performing tests at a frequency of 9 Hz [16] in a laminate which contains 43 % of it's plies in the  $0^\circ$  direction, hysteresis heating is not expected due to the small strain experienced by the material. Ryder [10] found that an  $8^\circ\text{C}$  temperature rise was typical late in the life of a fatigue test as a result of delamination which was introduced during testing. Since a  $10^\circ\text{C}$  temperature rise was experienced early in the life of the specimen, it appears that the delamination began at the onset of testing.

Some interesting observations are drawn from the SEM pictures. Note the dark gaps on the high head surface (Fig. 44) as compared with the low head rate tensile test (Fig. 45). These gaps represent a less uniform fracture surface or a wider zone of failure.



A close-up detail of the fiber (Fig. 48) shows typical brittle fracture at the fiber ends. From the fiber detail the small bumps which are attached to the fiber appear to be either fiber defects [31] or debris. However, it is more likely that the bumps are debris associated with the fracture. When considering the question of why the residual strength increased, some intriguing observations are drawn from Figs. 49 and 50 where samples produced an increase in residual strength. The damage is clearly interlaminar. As seen in Fig. 50, which was fatigued for over a million cycles, ply separation is clearly visible. In fact, after close examination, the ply separations occur around the  $\pm 45^\circ$  plies. The same observation of ply separations near  $\pm 45^\circ$  plies is made from Fig. 52. In contrast, a specimen which did not receive a long fatigue history (Fig. 49) does not show the same signs of ply separation. It should also be noted that no noticeable ply separations were seen on SEM pictures of samples which did not receive a fatigue history. Thus it is concluded that machining delamination occurred at the specimen's entry and exit but not through the entire laminate thickness.

From Fig. 30 it is clear that the residual strength increases after cyclic loading. Figures 32 and 34 demonstrate that the residual strength increase is a function of both cyclic load level during fatigue testing and the head rate at which the residual strength testing is performed. From Fig. 35, the slopes of the lines are similar, suggesting that the level of prior drilling damage does not change the degree to which the residual strength increases.

The clearly evident increase in residual strength may be a result of a combination of mechanisms. It is possible that the increase is due to progressive removal of the stress

concentration effect of the hole. However, Ramani [11] concluded that the hole plays a passive role in the mechanics of failure in graphite epoxy panels. Sendeckj [25] speculated from testing with notched specimens that any increase in residual strength was due to matrix damage. From his study he concludes that residual strength increases when the size of the fatigued induced matrix zone is much larger than the delamination zone found in static tests. Therefore, the fatigue process increases the delamination zone around the hole.

Combining the observations and results obtained from the present study of a graphite/epoxy specimen with a central hole with previous similar research, the following theory explaining the residual strength increase is mentioned. The increase in residual strength is indeed related to matrix damage, as Sendeckj concludes, and it occurs from damage which propagates during fatigue testing. Delaminations which were acquired by the specimen during machining spread during fatigue testing. This delamination spread is documented by the temperature rise which occurred early during fatigue testing. From the SEM pictures the delaminations were between the  $\pm 45^\circ$  plies. Therefore, these plies are no longer constrained by the matrix. Perhaps this ply separation allows slight fiber alignment of the  $\pm 45^\circ$  plies during residual strength testing. This alignment would account for the increase in residual strength. It was also documented that the residual strength increased as the head rate increased. At a faster head rate it is conceivable that the speed increase would further align the  $45^\circ$  fibers.

## CHAPTER 6

### CONCLUSIONS AND RECOMMENDATIONS

#### Conclusions

The  $[(\pm 45/0/90/0)_2 / \bar{0}]_s$  graphite epoxy laminate had a tensile strength of 30 KN and a strain which was 1.04% of the gauge length. As a result of this investigation, I conclude:

1. The split point carbide bit produced less damage then the conventional HSS bit at all of the feed rates.
2. Machining delamination occurred at the entry and exit but not necessarily through the thickness of the laminate.
3. The tensile strength of the graphite/epoxy laminate is not affected by differing feed or head rates.
4. Comparison between thermoset and thermoplastic matrices reveals that head rate has a greater effect on thermoplastics than thermosets. The difference is probably due to the viscoelastic nature of each of the matrices.

5. This graphite epoxy laminate is highly fatigue resistant even when damaged.
6. Based upon the 9 °C temperature rise, fatigue testing delamination began at the onset of testing.
7. Interlaminar damage in the form of ply separation accumulated around the  $\pm 45^\circ$  plies of the  $[(\pm 45/0/90/0)_2 / \bar{0}]_s$  graphite/epoxy laminate during fatigue testing.
8. Axial tension-tension fatigue testing increased the residual strength of the  $[(\pm 45/0/90/0)_2 / \bar{0}]_s$  graphite/epoxy laminate. As both the cyclic load level and head rate increased the residual strength increased. The degree of prior drilling damage did not have any effect on the residual strength.
9. The increase in residual strength is believed to be due to matrix damage around the  $\pm 45^\circ$  plies. The separated  $\pm 45^\circ$  plies, which are no longer constrained by the matrix, align during residual strength testing.

### Recommendations

1. Study the effect of damage accumulation and residual strength testing on other comparable composite systems.
2. Alter the frequency of the fatigue testing to determine frequency effects on the residual strength of the material.
3. Study the damage accumulation through the use of non-destructive testing techniques such as X-radiograph and acoustic emissions.
4. Explore the use of resin injection techniques on graphite epoxy as a means to alter fatigue life and residual strength.
5. Investigate the effect of other tool designs on damage accumulation and strength testing.

## REFERENCES

1. Wolterman, R. L., Kennedy, J. M., and Farley, G. L., "**Fatigue Damage in Thick, Cross-ply Laminates with a Center Hole**," *Composite Materials, Fatigue and Fracture, Fourth Volume*, ASTM STP 1156, W.W. Stinchcomb and N.E. Ashbaugh, Eds., American Society for Testing and Materials, 1993, pp. 473-490.
2. Ho-Cheng, H., and Daran, C. K. H., "**Delamination During Drilling in Composite Laminates**," *ASME Journal of Engineering for Industry*, Aug., Vol. 112, 1990, pp. 236-239.
3. Rosen, B.W., "**Analysis of Material Properties**," *Engineering Materials Handbook: COMPOSITES*, American Society for Metals, Vol. 1, 1987, p. 203.
4. Jain, S. and Yang, D.C.H., "**Effects of Feed Rate and Chisel Edge on Delamination in Composite Drilling**," *ASME Journal of Engineering for Industry*, Nov., Vol. 115, 1993, pp. 398-405.
5. Pengra, J.J., and Wood, R.E., "**The Influence of Hole Quality on Graphite Epoxy Composite Laminates**," collective technical papers, AIAA, ASME, ASCE, AHS, *21st Structures and Structural Dynamics Material Conference*, AIAA paper 80-0777, 1980, pp. 687-693.
6. Andrews, S.D., Ochoa, O.O., and Owens, S.D., "**Recent Advances in Structural Mechanics**," ASME PVP-vol. 225/NE-Vol. 7, 1991, pp. 51-56.
7. Hegde, A., "**Investigation of Drilling Induced Damage In PPS/Glass Fiber Reinforced Composites**," *Masters of Science Thesis*, Oklahoma State University, 1995, p. 54.
8. Kam, C.Y., "**Bolt Hole Growth in Graphite-Epoxy Laminates for Clearance and Interference Fits When Subjected to Fatigue Loads**," *Fatigue of Fibrous Composite Materials*, ASTM STP 723, American Society for Testing and Materials, 1981, pp. 21-30.

9. Chang, F.H., Gordon, D.E., and Gardner, A.H., "**A Study of Fatigue Damage in Composites by Nondestructive Testing Techniques**," *Fatigue of Filamentary Composite Materials*, ASTM STP 636, K.L. Reifsnider and K.N. Lauraitis, Eds., American Society for Testing and Materials, 1977, pp. 57-72.
10. Ryder, J.T. and Walker, E.K., "**Effect of Compression on Fatigue Properties of a Quasi-Isotropic Graphite/Epoxy Composite**," *Fatigue of Filamentary Composite Materials*, ASTM STP 636, K.L. Reifsnider and K.N. Lauraitis, Eds., American Society for Testing and Materials, 1977, pp. 3-26.
11. Ramani, S.V. and Williams, D.P., "**Notched and Unnotched Fatigue Behavior of Angle-Ply Graphite/Epoxy Composites**," *Fatigue of Filamentary Composite Materials*, ASTM STP 636, K.L. Reifsnider and K.N. Lauraitis, Eds., American Society for Testing and Materials, 1977, pp. 27-46.
12. Lee, J.H. and Mall, S., "**Strength of Composite Laminate with Reinforced Hole**," *Journal of Composite Materials*, April, Vol. 23, 1989, pp. 337-347.
13. Hocheng, H., Pwu, H.Y., and Yao, K.C., "**Machinability of some Fiber Reinforced Thermoset and Thermoplastics in Drilling**," *Material and Manufacturing Processes*, 1993, pp. 653-682.
14. Colligan, K. and Ramulu, M., "**An Experimental Investigation Into Pitting of Hole Surfaces when Drilling Graphite/Epoxy Materials**," *Processing, Fabrication, and Manufacturing of Composites Materials*, American Society of Mechanical Engineers, MD-Vol. 35, 1992, pp. 11-25.
15. Butler, R.J., Bernard, P.M., and Curtis, P.T., "**The Development of a Satisfactory, Simple, Shear Fatigue Test for Unidirectional E-Glass Epoxy**," ASTM STP, 1986.
16. Curtis, P.T., "**The Fatigue Behavior of Fibrous Composite Materials**," *Journal of Strain Analysis*, Vol. 24, no. 4, 1989, pp. 47-56.
17. Kim, R.Y., "**Fatigue Strength**," *Engineering Materials Handbook: COMPOSITES*, American Society for Metals, Vol. 1., 1987, pp. 436-441.
18. Masters, J.E., "**Basic Failure Modes of Continuous Fiber Composites**," *Engineering Materials Handbook: COMPOSITES*, American Society for Metals, Vol. 1, 1987, pp. 781-783.
19. Walter, R.W., Johnson, R.W., June, R.R. and McCarty, J.E., "**Designing for Integrity in Long-Life Composite Aircraft Structures**," *Fatigue of Filamentary Composite Materials*, ASTM STP 636, K.L. Reifsnider and K.N. Lauraitis, Eds., American Society for Testing and Materials, 1977, p. 243.

20. Smith, B.W., **"Fractography for Continuous Fiber Composites,"** *Engineering Materials Handbook: COMPOSITES*, American Society for Metals, Vol. 1, 1987, pp. 786.
21. Nayak, P. **"Tensile and Fatigue Behavior of Woven-Glass Fiber Reinforced Polyphenylene Sulfide Composite laminates,"** *Creative Component*, Oklahoma State University, 1990.
22. Powers, L.T., **"Uniaxial Tension Fatigue of Woven-Glass Fiber Reinforced Polyphenylene Sulfide Composite with Circular Hole,"** *Creative Component*, Oklahoma State University, 1992.
23. Schutz, D., Gerharz, J.J. and Alschweig, E., **"Fatigue Properties of Unnotched, Notched, and Joint Specimens of a Graphite/Epoxy Composite,"** *Fatigue of Fibrous Composite Materials*, ASTM STP 723, American Society for Testing and Materials, 1981, pp. 31-47.
24. Elahi, M., Razvan, A. and Reifsnider, K.L., **"Characterization of Composite Material's Dynamic Response Using Load/Stroke Frequency Response Measurement,"** *Composite Materials, Fatigue and Fracture, Fourth Volume*, ASTM STP 1156, W.W. Stinchcomb and N.E. Ashbaugh, Eds., American Society for Testing and Materials, 1993, pp. 575-588.
25. Sendeckyj, G.P., Stalnaker, H.D. and Kleismit, R.A., **"Effect of Temperature on Fatigue Response of Surface-Notched [(0/±45/0)<sub>s</sub>]<sub>3</sub> Graphite/Epoxy Laminate,"** *Fatigue of Filamentary Composite Materials*, ASTM STP 636, K.L. Reifsnider and K.N. Lauraitis, Eds., American Society for Testing and Materials, 1977, p 136.
26. Awerbuch, J. and Hahn, H.T., **"Off-Axis Fatigue of Graphite/Epoxy Composite,"** *Fatigue of Fibrous Composite Materials*, ASTM STP 723, American Society for Testing and Materials, 1981, pp. 257-260.
27. Gibson, R.F., *Principles of Composite Material Mechanics*, McGraw-Hill, Inc., 1994, pp. 81-82, 207-213.
28. *Engineers Guide to Composite Materials*, American Society for Metals, 1987, p. 5-9.
29. Mackey, B.A. Jr., **"How to Drill Precision Holes in Reinforced Plastics in a Hurry,"** *Plastics Engineering*, Vol. 36, no. 2, Feb., 1980, p.23.
30. Stinchcomb, W.W., Reifsnider, K.L., Yeung, P. and Masters J., **"Effect of Ply Constraint on Fatigue Damage Development in Composite Material Laminates,"**



*Fatigue of Fibrous Composite Materials*, ASTM STP 723, American Society for Testing and Materials, 1981, p. 67.

31. Donnet, J-B., Bansal, R.C., *Carbon Fibers*, Marcel Dekker, Inc., 1984.

## APPENDIX A--TESTING SUMMARY

Sample	Test Information T - Tensile; R - Residual Type - # of cycles - max cyclic load T or R - N - KN (lb)	Head Rate mm/s (in/s)	Load KN (lb)	Notes
H1-A-1	R - 7500 - 26.7 (6000)	20.3 (0.8)	33.2 (7462)	a
H1-A-2	T	.051 (.002)	29.8 (6700)	
H1-A-3	R - 100,006 - 27.9 (6275)	.051 (.002)	32.6 (7321)	
H1-A-4	R - 100,690 - 22.2 (5000)	.051 (.002)	33.8 (7597)	b
H1-B-5	R - 10,007 - 27.9 (6275)	.051 (.002)	32.6 (7331)	
H2-B-7	T	.051 (.002)	29.8 (6704)	
H3-C-8	R - 199,596 - 25.9 (5830)	20.3 (0.8)	35.7 (8020)	a
H3-C-9	T	.203 (.008)	30.6 (6870)	
H3-C-10	R - 1,150,855 - 27.9 (6275)	.051 (.002)	37.2 (8359)	
H4-D-12	R - 10,010 - 27.9 (6275)	.051 (.002)	32 (7200)	
H4-D-13	T	.051 (.002)	29.9 (6730)	
H4-D-14	T	.051 (.002)	31.3 (7036)	c
H5-E-15	R - 10,010 - 27.9 (6275)	.051 (.002)	32.9 (7404)	
H5-E-17	T	.051 (.002)	29.6 (6662)	
C1-C-21	R - 10,005 - 27.9 (6275)	.051 (.002)	32.7 (7358)	
H6-C-24	T	.013 (.0005)	29.9 (6722)	
H6-C-25	T	.051 (.002)	29.9 (6719)	
H6-C-26	T	.13 (.005)	30.5 (6848)	
H6-C-27	T	.004 (.00015)	29.7 (6685)	
H7-C-28	T	20.3 (0.8)	30.0 (6739)	
H7-C-29	R - 1,100,000 - 27.9 (6275)	.051 (.002)	36.1 (8124)	
H7-C-30	R - 1,100 - 27.9(6275)	.051 (.002)	32.7 (7354)	e
H7-C-31	R - 150 - 27.9 (6275)	.051 (.002)	30.7 (6900)	e
H8-C-32	R - 10,008 - 27.9 (6275)	.051 (.002)	33.2 (7472)	
H8-C-33	R - 10,006 - 24.0 (5403)	.051 (.002)	32.6 (7327)	
H8-C-34	R - 10,008 - 21.0 (4725)	.051 (.002)	30.9 (6947)	
H8-C-35	R - 380,006 - 27.9 (6275)	.051 (.002)	33.7 (7585)	d
H9-C-36	R - 10,005 - 27.9 (6275)	.013 (.0005)	32.2 (7247)	d
H9-C-37	R - 10,007 - 27.9 (6275)	13.5 (.53)	32.9 (7392)	d
H9-C-38	R - 290,005 - 27.9 (6275)	13.5 (.53)	35.6 (8005)	
H9-C-39	R - 290,006 - 27.9 (6275)	.013 (.0005)	33.9 (7621)	
C1-A-41	T	.25 (.01)	29.8 (6700)	

Notes: a - Operator error led to unintentional tensile test  
b - Test partially performed at displacement control  
c - load value is higher then expected; not used as valid data  
d - Temp data recorded  
e - 100 cycles were deducted from the total # of cycles

2  
VITA

John W Wedeking

Candidate for the Degree of

Master of Science

Thesis: MACHINING EFFECTS ON TENSILE AND FATIGUE BEHAVIOR  
IN A  $[(\pm 45/0/90/0)_2/\bar{0}]_s$  GRAPHITE EPOXY LAMINATE

Major Field: Mechanical Engineering

Biographical:

Personal Data: Born in Grand Forks, North Dakota, On July 12, 1970, the son of David and Susan Wedeking.

Education: Graduated from Putnam City West High School, Oklahoma City, Oklahoma in May 1988. received Bachelor of Science Degree in Mechanical Engineering from Oklahoma State University, Stillwater, Oklahoma in December 1993. Completed the requirements for the Master of Science degree with a major in Mechanical Engineering at Oklahoma State University in December 1995.

Experience: Employed by Dow Chemical Company, Freeport, Texas as an alternating term co-op for three semesters. Employed by Oklahoma State University, Department of Mechanical and Aerospace Engineering as a Graduate Teaching Assistant from January 1994 to May 1995.

Professional Memberships: American Society of Mechanical Engineers, American Society of Heating, Refrigeration and Air-conditioning Engineers, Pi Tau Sigma.